DNA 4334F

ANALYSIS AND DESIGN OF A TWO-STAGE HYBRID LAUNCHER

Acurex Corporation
485 Clyde Avenue
Mountain View, California 94042

May 1977

Final Report for Period 15 January 1977—30 July 1977

CONTRACT No. DNA 001-76-C-0407

THIS WORK SPONSORED BY THE DEFENSE NUCLEAR AGENCY
UNDER RDT&E RMSS CODE B342077464 N99QAXAA12949 H2590D.

Prepared for
Director
DEFENSE NUCLEAR AGENCY
Washington, D. C. 20305

UNCLASSIFIED

SECURITY CLASSIFICATION OF THIS PAGE (When Data Entered)

REPORT DOCUMENTATION PAGE

READ INSTRUCTIONS BEFORE COMPLETING FORM

1. REPORT NUMBER: DNA 4334F
2. GOVT ACCESSION NO.
3. RECIPIENT'S CATALOG NUMBER

4. TITLE (and Subtitle): ANALYSIS AND DESIGN OF A TWO-STAGE HYBRID LAUNCHER.

5. TYPE OF REPORT & PERIOD COVERED: Final Report for Period 15 Jan [illegible] — 30 Jul 77

6. PERFORMING ORG. REPORT NUMBER: TR-77-245 (726[illegible])

7. AUTHOR(s): T. J./Dahm, J. D./Watson

8. CONTRACT OR GRANT NUMBER(s): DNA 001-76-C-0407

9. PERFORMING ORGANIZATION NAME AND ADDRESS: Acurex Corporation, 485 Clyde Avenue, Mountain View, California 94042

10. PROGRAM ELEMENT, PROJECT, TASK AREA & WORK UNIT NUMBERS: Subtask N99QAXAA129[illegible]49

11. CONTROLLING OFFICE NAME AND ADDRESS: Director, Defense Nuclear Agency, Washington, D.C. 20305

12. REPORT DATE: May [illegible]77

13. NUMBER OF PAGES: 86

14. MONITORING AGENCY NAME & ADDRESS (if different from Controlling Office): DNA, SBIE

15. SECURITY CLASS (of this report): UNCLASSIFIED

15a. DECLASSIFICATION/DOWNGRADING SCHEDULE

16. DISTRIBUTION STATEMENT (of this Report)

Approved for public release; distribution unlimited.

17. DISTRIBUTION STATEMENT (of the abstract entered in Block 20, if different from Report)

18. SUPPLEMENTARY NOTES

This work sponsored by the Defense Nuclear Agency under RDT&E RMSS Code B342077464 N99QAXAA12949 H2590D.

19. KEY WORDS (Continue on reverse side if necessary and identify by block number)

Hypervelocity Launcher
Reentry Vehicle Simulation
Light Gas Gun
Projectile
Ballistic Heat Transfer

20. ABSTRACT (Continue on reverse side if necessary and identify by block number)

This report summarizes the analysis and design of a two-stage hybrid launcher capable of soft launching 12-pound, 4-inch diameter models to 20000 fps. The design and configuration of explosive drivers to inject high energy hydrogen into the compressor section of a two-stage gun is described. The calculation of ballistic performance is of note. The detailed calculation of inviscid, adiabatic core flow in conjunction with an analysis of launch tube

DD FORM 1 JAN 73 1473 EDITION OF 1 NOV 65 IS OBSOLETE

UNCLASSIFIED

SECURITY CLASSIFICATION OF THIS PAGE (When Data Entered)

409 549

SUMMARY

This report describes the analysis and design of a hybrid launcher of greatly improved ballistic efficiency, suitable for testing high-β full-scale nosetips in an extended track range facility. Two key launcher design problems have been analyzed and solved. A design and configuration of explosive drivers has been developed to inject sufficient hydrogen into the compressor section of the launcher with a minimum of gas loss. A thermal liner composite of tungsten and tantalum carbide has been designed to withstand the high heat loads during compression without melting. As a result, a practical ballistic cycle has been developed to accelerate a 4-inch diameter, 10-pound fragile model to 20000 fps without exceeding 5 kilobars on the model or melting the interior of the launcher. By using a larger launch tube and saboting the model, an alternate ballistic cycle has been devised to increase the launch mass to 12 pounds while simultaneously reducing the peak reservoir pressures and temperatures. The design for a 1/4-scale hybrid launcher to demonstrate these ballistic cycles has been completed.

PREFACE

The authors wish to acknowledge the valuable contributions of Dr. Dennis Baum (Artec Associates, Inc.) to the design of the explosive drivers and the injection block.

TABLE OF CONTENTS

TABLE OF CONTENTS (Concluded)

LIST OF ILLUSTRATIONS

LIST OF ILLUSTRATIONS (Concluded)

SECTION 1

INTRODUCTION

In principle a hypervelocity launcher can be designed on a large enough scale to permit testing of full-scale reentry vehicles in a ground-based facility. Such a launcher, based on the straightforward application of conventional two-stage light gas gun technology would be extremely costly. Furthermore, a gun of such size would require development of new fabrication techniques and would not be without risk.

One of several alternative approaches to ground-based reentry testing is to develop a launcher of greatly improved ballistic efficiency and utilize it on a more modest scale to test high-β full-scale nosetips in an extended track range facility. Such an approach would not be prohibitively expensive and could substantially extend test times to provide high-quality erosion/ablation data.

This report describes the design of a hybrid launcher capable of soft-launching a model two to three times more massive than can be propelled by a conventional two-stage gun of the same bore.

The hybrid launcher utilizes several explosive drivers to precondition and inject high-energy hydrogen into the compressor section of a two-stage light gas gun. As a result, maximum tolerable pressures and temperatures can be developed with a very short compression cycle. Furthermore, the pressure history can be controlled independently of the peak reservoir gas temperature making possible a very efficient ballistic cycle for accelerating high-β models.

The basic concept of the hybrid launcher is not new. Attempts in Reference 1 to demonstrate such a launcher in subscale were not successful —

launcher velocities were considerably below expectations. A number of reasons for this performance shortfall were identified in Reference 2. In brief, these are:

- The design relied on projectile acceleration at high launch tube length to diameter ratios, without consideration for heat transfer and boundary layer effects
- The design ratio of gas to projectile mass was too low and, in addition, a large fraction of gas failed to be injected into the compressor section due to choking and the injection configuration
- The first stage 75-mm gun had insufficient energy to achieve the design muzzle velocity with the proper launch tube length
- Melting occurred in the compressor section and launch tube
- The explosive drivers were overcharged, causing driver jetting and contamination of the working gas

The authors of Reference 2 conclude that the basic concept does have considerable merit and is feasible with modifications to the design. In the revised design reported herein, the injection scheme has been reconfigured to minimize injection losses. The explosive drivers have been redesigned to inject substantially more gas and the ballistic cycle design calculations have been carried out within a more practical performance envelope.

The use of thermal liners in critical areas of the gun is the key to exploiting the high temperatures generated in the hybrid launch cycle. With practical material strategies, temperatures in excess of 5800°K can be utilized without melting the interior of the gun.

The high-performance ballistic cycle described herein is designed to accelerate 10-pound, 4-inch diameter models to 20000 fps.

The launch mass-velocity of the model can be further increased or the peak reservoir conditions can be relaxed by using a larger or superbored launch tube. However, special sabot stripping techniques must be developed to couple a superbore launcher with a track-guided range facility.

Engineering drawings of a 1/4-scale hybrid launcher have been made on the basis of the above analytical work. This design, which can be converted easily to a superbore configuration, is recommended for building and testing.

SECTION 2

DESIGN OF THE BALLISTIC CYCLE

The objective of this analysis is to recommend the best approach for launching the highest possible mass to a velocity of 20000 fps (6.1 km/sec). The minimum specific goal is to accelerate a 10-pound, 4-inch diameter model to 6.1 km/sec within the constraints outlined below.

2.1 DESIGN CONSTRAINTS

The design of a gun to launch high-β models is limited to a performance envelope defined by several launcher and model material limits. In particular, the maximum pressure on the base of the model is limited to 5 kilobars, a limit imposed largely by the experience gained launching unsaboted nosetip models in conventional two-stage light gas guns. The design is also constrained to a maximum launch tube length of 300 bore diameters as a result of experimental and theoretical work which indicates that performance gains are marginal after approximately 300 diameters of travel.

Under these two constraints, the maximum possible muzzle velocity for a 10-pound model in a 4-inch diameter launch tube is 7.38 km/sec with an idealized constant base pressure launch cycle.* The design velocity of 6.1 km/sec is, thus, 83 percent of the maximum possible velocity and would

---

*For a constant base pressure, p, the model velocity, u, is given by:

$$u = \left[\frac{2pAx}{m}\right]^{1/2}$$

where A = bore cross section
x = launch tube length
m = model mass

require an average model base pressure of 3.47 kilobars during the launch cycle. Since the maximum allowable base pressure is 5 kilobars, the piezometric efficiency* of the ballistic cycle must be 70 percent or more.

Such an efficient ballistic cycle requires a working fluid with the highest possible sound speed. Hydrogen offers the best combination of high sound speed and low heat transfer properties. The maximum heat load that can be tolerated in the interior of the gun limits the peak temperatures and, hence, sound speeds that can be generated during the ballistic cycle. As will be detailed later, the practical limit on peak reservoir temperature for tungsten, tantalum carbide lined barrels appears to be about 5800°K.

An extended barrel 16-inch Naval gun is the largest available hardware† for use as a first stage to drive a 10-pound model in a 4-inch launch tube. This establishes an upper limit on pistor energy (~400 million foot-lbs) and piston velocity (~8000 fps).

For a compressor section of this size, the peak reservoir pressures are limited to about 8 kilobars within the cost-effective choices of available materials, fabrication techniques and heat treats.

In summary, the major design constraints are taken as:

- 5-kb maximum model base pressure
- 300-bore diameter launch tube
- 5800°K maximum reservoir temperature
- 16-inch Naval gun first stage driving a 4-inch launch tube
- 8-kb maximum reservoir pressure

---

*The piezometric efficiency is defined as:

$$\mathbb{P} = \frac{\text{constant base pressure to give the observed velocity}}{\text{peak base pressure generated during the ballistic cycle}}$$

†For example, the U.S. Army has a double length barrel (120 feet) 16-inch gun used for high altitude firings at Yuma, Arizona. A larger first stage can always be manufactured at substantial extra cost.

To account for heat transfer losses, boundary layer losses, etc., a minimum muzzle velocity of 6.7 km/sec for the calculated ballistic cycle is considered necessary to provide about a 10-percent margin over the 6.1 km/sec design velocity.

2.2 DESIGN OPTIONS

Four approaches were considered to achieve the ballistic cycle efficiency that satisfies the aforementioned design constraints. These were:

- Injection of high energy gas along the launch tube
- A high energy preburned propellant gun
- An optimized conventional two-stage light gas gun
- A hybrid two-stage light gas gun

Injection of gas at several positions along the launch tube is in principle feasible using either small explosive drivers or liquid propellant actuated devices. Both methods are capable of injecting high energy gas within a few diameters of the accelerating model and with the necessary timing accuracy. However, both methods involve a number of complex technical problems and developmental risks. These techniques may be reconsidered if even higher muzzle velocities or model weights are required.

A high energy preburned propellant ballistic cycle was considered in which explosive drivers would be used to create a reservoir of high pressure, high temperature hydrogen. Here, peak reservoir temperatures would be again limited by heat transfer to about 5800°K. However, in the preburned propellant mode, peak reservoir pressure would be limited to the peak model base pressure of 5 kilobars.

Using a Seigel calculation (Reference 3) for an effectively infinite reservoir of 5-kb real hydrogen at 5800°K,* the calculated muzzle velocity

---

*For real hydrogen at 5 kb and 5800°K, the density is 0.016 gm/cm^3, the sound speed is 6.6 km/sec and the isentropic index, γ, is 1.42 (see Appendix A, Reference 2).

is 5.8 km/sec which is below the design velocity of 6.1 km/sec and considerably short of the calculational performance goal of 6.7 km/sec necessary to accommodate expected heat transfer and boundary layer losses.

An optimized two-stage light gas gun utilizing a 16-inch Naval gun as the first stage was considered. To achieve maximum tolerable pressures and temperatures (8 kilobars and 5800°K respectively) with an isentropic compression cycle would require an impossibly long pump tube (16-inch diameter by 14 miles long). The combination of a reasonably long pump tube and an 8000 fps piston in a shock heated compression cycle is still unable to generate peak temperatures much in excess of 2000°K without overpressuring both the reservoir and model. That is, the piston is not fast enough to provide the necessary shock heating but too fast to allow proper matching of reservoir pressure buildup with the acceleration of the high-β model. A conventional two-stage light gas gun of practical size is therefore not suitable for launching high-β models to the required velocities under the current design constraints.

The injected or hybrid two-stage launcher however avoids this dilemma by using the first-stage piston primarily to control the rate of reservoir pressure buildup to provide an approximately constant base pressure on the model.

The proper state of the hydrogen to achieve maximum tolerable reservoir pressure and temperatures is controlled primarily by the explosive drivers. Thus, the state of the gas and the rate of reservoir pressure buildup are independently controlled.

2.3 HYBRID LAUNCHER DESIGN PRINCIPLES

Explosive drivers are used to process the hydrogen to a high energy density state by a single strong shock. The gas is then injected into the compressor section. This injected state (prior to compression) is characterized by its energy density which is a function of the $p\Delta V$ work of the drivers and by its mass density which is a function of the injection volume. The injection state for a given mass, G, of gas is thus:

$$\left.\begin{aligned} e_{inj} &= \frac{5/2RT_o + p_2\Delta V}{G} \\ \rho_{inj} &= \frac{G}{V_{inj}} \end{aligned}\right\} \qquad (1)$$

where T_o = ambient temperature at loading

p_2 = explosive driver shocked gas pressure

ΔV = change in volume of drivers during operation

V_{inj} = compressor volume just after injection port closure

Compression to final reservoir conditions is very nearly isentropic and the energy of the gas is increased by the piston as it decelerates to rest. If the model is restrained, the peak reservoir conditions are given by:

$$e_{max} = \frac{5/2RT_o + p_2\Delta V + (1/2MU^2)_{pist}}{G}$$

$$(S/R)_{max} = (S/R)_{inj} \qquad (2)$$

where M = piston mass

U = piston velocity

S/R = dimensionless entropy

A modified Mollier diagram (e versus S/R) for real hydrogen is shown in Figure 1. Typical compression cycles for a shock heated conventional two-stage gun and a hybrid two-stage gun are included to illustrate the advantage of the hybrid concept. These examples are illustrative of a conventional two-stage gun and a hybrid launcher of approximately the same size. The conventional two-stage gun shown has a 16-inch diameter by 225-foot long pump tube and the hybrid launcher has a 16-inch diameter by 153-foot long first-stage compressor section. It is clear that the size of the conventional two-stage gun would have to be increased to an impractical value to achieve the same high energy reservoir states as the hybrid launcher.

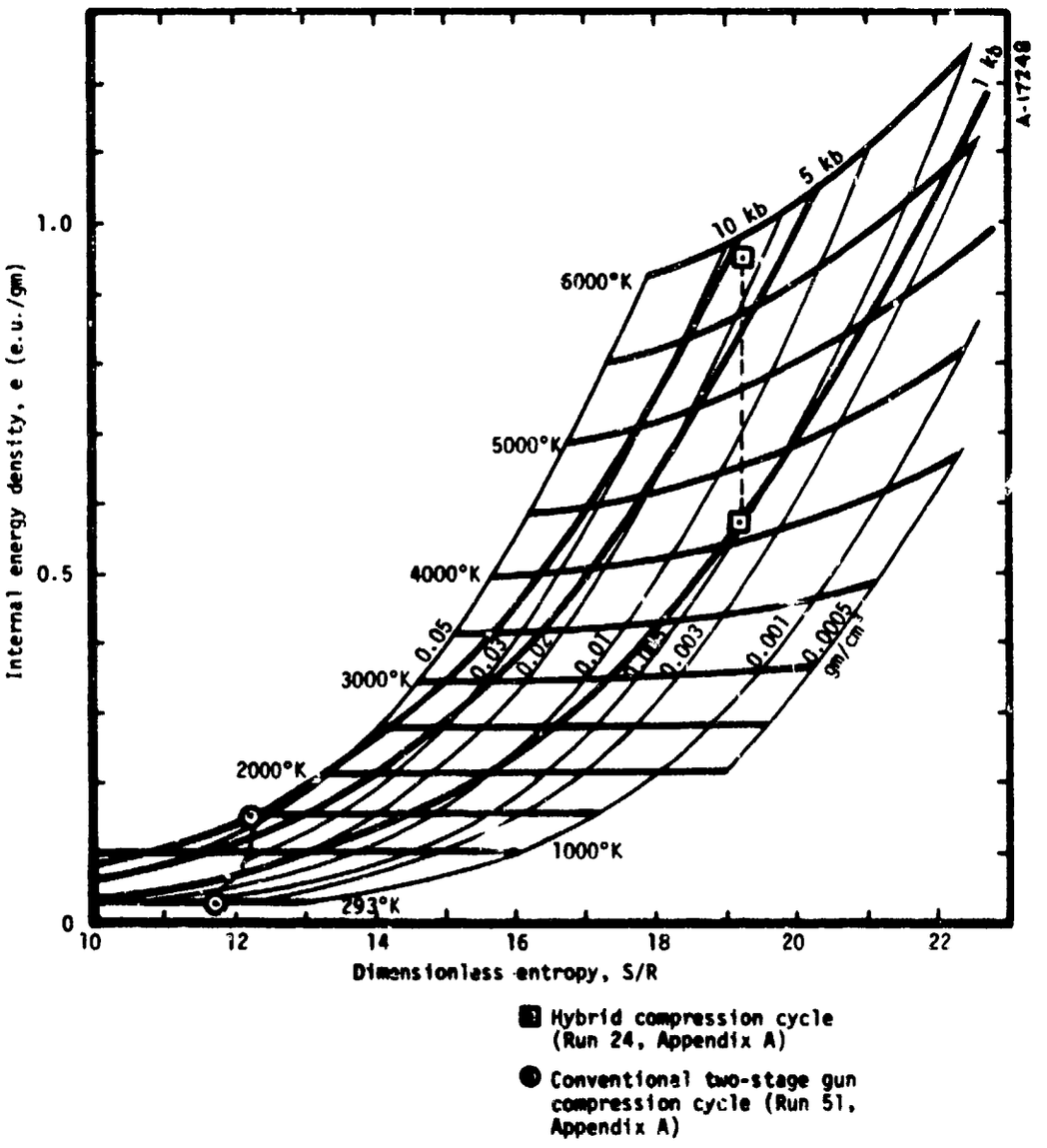

Figure 1. Modified Mollier diagram for real hydrogen showing conventional and hybrid compression cycles.

The energy of the gas in the conventional cycle is completely controlled by piston energy whereas for the hybrid cycle about 60 percent of the energy of the gas is provided by the explosive drivers and 40 percent by the piston. Thus, for the same size first-stage, the hybrid launcher has substantially more energy available in addition to having independent control over the state of the gas and the rate of reservoir pressure buildup.

The maximum tolerable reservoir pressure and temperature which in practice peak simultaneously, occur at a unique entropy level. For example, from Figure 1, the dimensionless entropy, S/R, is 19.25 at 8 kilobars and 5000°K. Since compression is approximately isentropic, the entropy at injection is also 19.25. Injection energy is controlled by the $p\Delta V$ work of the explosive drivers, so the compressor volume at injection which controls injection density is used to control the entropy level at which compression occurs. As will be described in the next section, injection volume (or piston position at injection) is used as the primary "thermostat" to control peak compression temperatures.

The operational sequence of the hybrid launcher is shown in Figure 2. In practice, the model begins to accelerate before the piston decelerates to rest and the maximum reservoir conditions predicted by Equation (2) are not quite reached.

2.4 HYBRID LAUNCHER DESIGN ANALYSIS

A 1-1/2 D Lagrangian finite difference code (the STEALTH code described in Reference 4) was used to compute the hybrid launcher inviscid, adiabatic ballistic cycle. The code includes a real hydrogen equation-of-state, area changes with one-dimensional gasdynamics and shot-start* condition. All the thermodynamic and gasdynamic variables, and piston and model trajectories are calculated as functions of time and position throughout the launch cycle.

*The shot-start condition is usually defined as the pressure at which the projectile is released from its initial position.

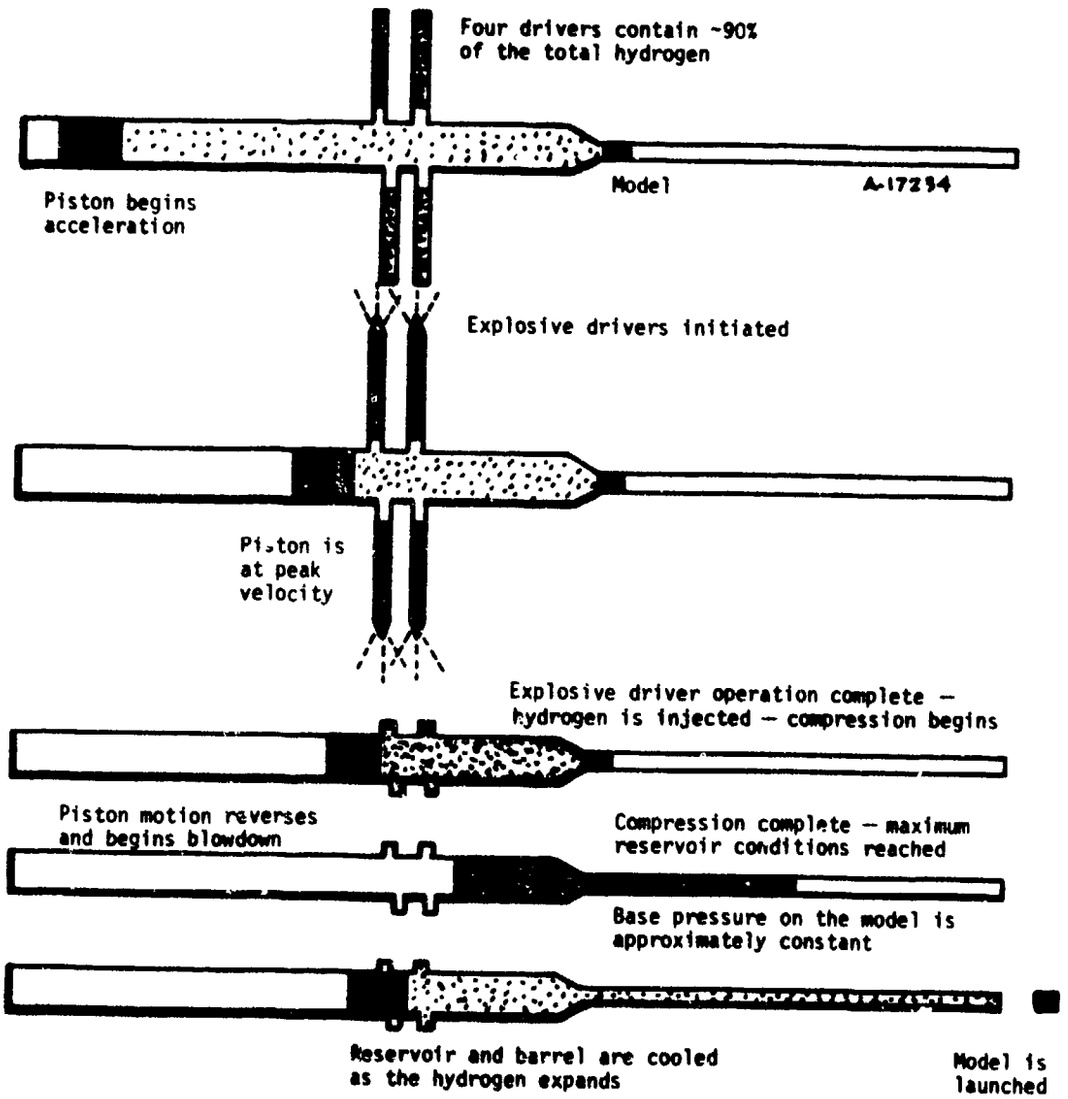

Figure 2. Operational sequence of the hybrid launcher.

The calculations were initialized to injection conditions defined by Equation (1) with the gas initially at rest* and the piston mass, M, at velocity, U, as shown schematically in Figure 3a.

Several launcher geometries, piston conditions, and initial gas conditions were evaluated in this manner to obtain the best performance within the design constraints. Once the most suitable combination of parameters was selected, the calculation was refined by initializing the calculations with a gas distribution more representative of the actual driver injection process (Figure 3b).

The calculations were carried out for a 1/4-scale of the full-scale launcher. Since the calculations assume inviscid adiabatic gas flow, results can be scaled by multiplying all times and lengths by the appropriate scale factor. The complete calculational matrix is summarized in Appendix A.

The calculations resulted in a selection of four launch cycle options which are summarized in Table 1 and described in the following sections.

2.4.1 86-gm Model, 1-inch Bore — Launch Cycle A

This launch cycle scales to a 12-pound model in a 4-inch bore launch tube and would use a 16-inch Naval gun as a first stage. For the 1/4-scale launcher, an M68 105-mm gun would be used for the first stage. The best calculated performance within the design constraints is a velocity of 6.0 km/sec with a 300-caliber launch tube. The corresponding reservoir pressure and temperature histories and the model base pressure history are shown in Figure 4.

The base pressure oscillations are real and are a result of low amplitude pressure waves in the reservoir being amplified by the 18:1 area change into the launch tube. Piston mass and velocity, injection volume and G/M ratio were varied to minimize these base pressure oscillations. The effect of more realistic initial gas distributions and shot-start conditions on the base pressure history is discussed below.

---

*In these calculations, the impact of the moving piston on the stationary gas is numerically very smooth and no numerical noise is generated.

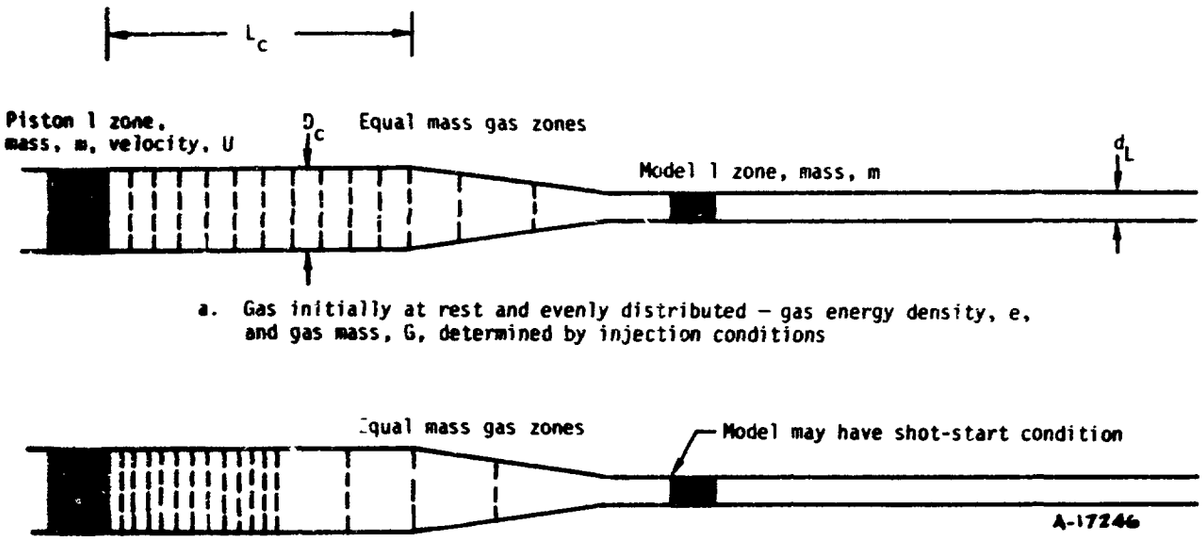

a. Gas initially at rest and evenly distributed – gas energy density, e, and gas mass, G, determined by injection conditions

b. Gas initially at rest with most of the gas in the injection block region of the compressor – gas energy density, e, and gas mass, G, determined by injection conditions

A summary of the ballistic cycle calculations is given in Appendix A.

Figure 3. Schematic of the STEALTH code 1-1/2-D ballistic cycle calculations.

TABLE 1. SUMMARY OF HYBRID LAUNCH CYCLE OPTIONS

Launch Cycle	Launch Tube Dia. (cm)	Model Mass (gms)	Piston Mass (lbs)	Piston Vel. (fps)	G/M	P_{max} Res. (kb)	T_{max} Res. (°K)	P_{max} Model (kb)	u_{300} (km/s)	u_{350} (km/s)	Full-Scale Launch Mass After Sabot Stripping (lbs)
A	2.54	86	12.5	4850	2	8.0	5700	5.2	6.0	6.5	12
B	2.54	72	11.5	5000	2	8.0	5840	5.2	6.5	7.0	10
C Superbore	3.175	112.5	14.0	5000	1.56	8.1	5710	5.3	7.1	7.6	12
D Relaxed Superbore	3.175	112.5	13.0	4800	1.56	6.6	5510	4.7	6.6	7.0	12

All four of the launch cycle options make use of the same first stage, injector, and compressor hardware.

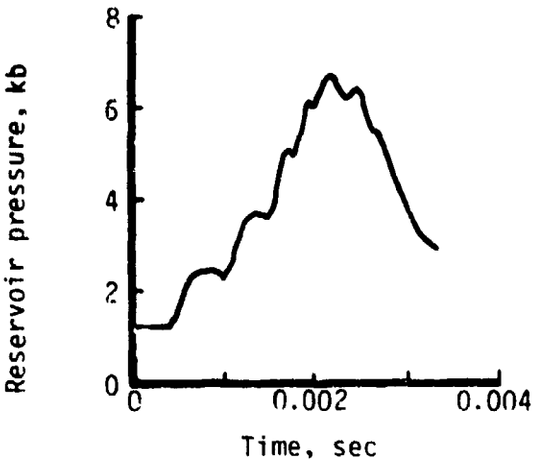

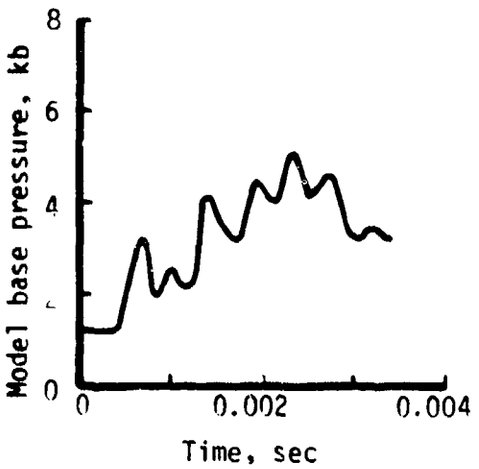

A-17250

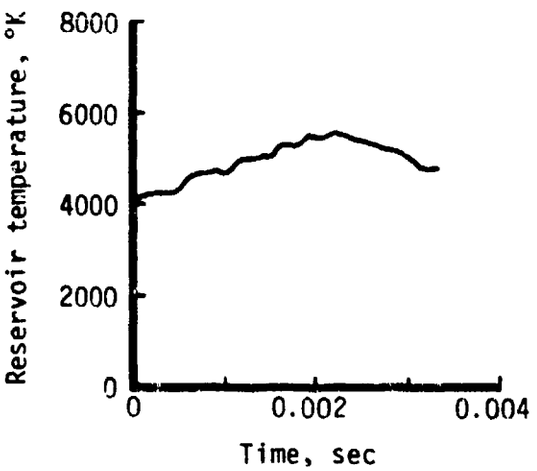

12-lb piston at 4850 fps
G/M = 2 L_C/D_C = 25
Total energy = 159 e.u.
u_{300} = 5.80 km/sec
u_{350} = 6.21 km/sec
(Run 6, Appendix A)

Reservoir conditions are taken at the throat entrance and are not necessarily maximum values

Figure 4. Calculated results for the 1-inch bore 86-gm model ballistic cycle.

2.4.2 72-gm Model, 1-inch Bore — Launch Cycle B

The only way to increase muzzle velocity without exceeding pressure and temperature limits and without increasing the bore of the launch tube is to reduce model mass. This launch cycle was chosen to scale to a minimum design 10-pound model in a 4-inch launch tube. The best calculated performance within design constraints is 6.5 km/sec with a 300-caliber launch tube. The corresponding reservoir pressure and temperature histories and the model base pressure history are shown in Figure 5. Calculated performance after 350 calibers is 6.9 km/sec and there is reason to expect to gain some of this extra performance with the high pressure, high sound speed hybrid launch cycle.*

Several pressure profiles are shown in Figure 6 at various times near the peak of the compression cycle. These pressure distributions, which extend from the face of the piston to the base of the model, clearly show the origin and progress of the pressure pulses as they are generated in the reservoir, amplified by the area change, and transmitted down the launch tube where they overtake the accelerating model.

This launch cycle appears to be able to deliver the required performance with a small performance margin to absorb some heat transfer and boundary layer losses. As will be discussed later, this launch cycle also requires special liner materials to tolerate the high heat loads generated during peak compression.

---

*The 300-caliber "limit" used in these performance calculations is based on the experience of conventional two-stage light gas gun work at considerably lower temperatures. As a result of the higher temperatures generated in the launch cycle of the hybrid gun, pressures in the launch tube are considerably higher. As pointed out in Reference 2, the boundary layer closure point would be moved further downstream. Thus, projectile acceleration could be expected to continue beyond 300 calibers of travel. The actual calibers of effective acceleration will of course have to be determined experimentally.

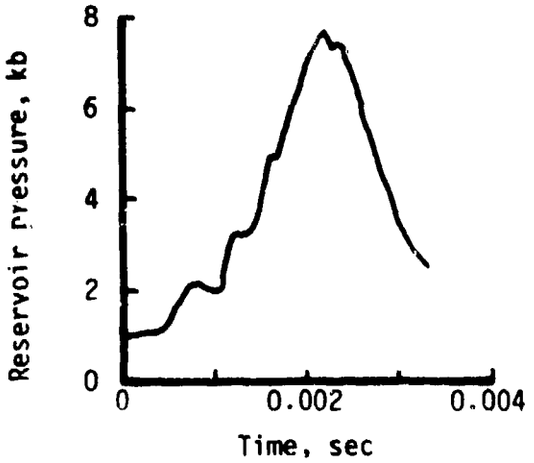

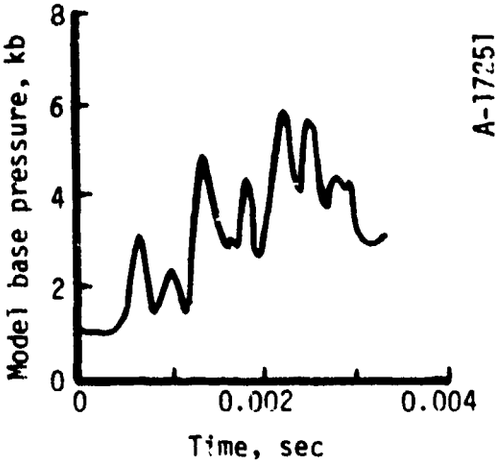

A-17251

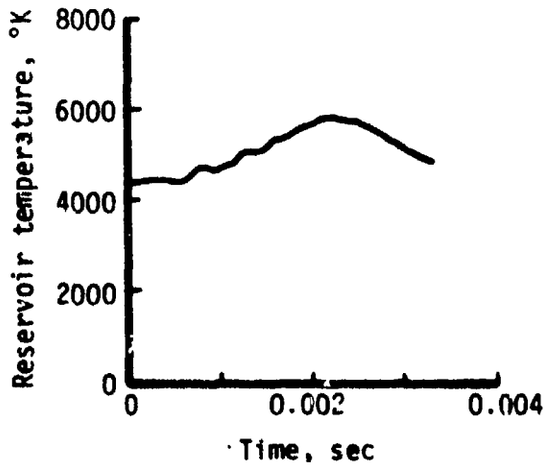

11.5-lb piston at 5000 fps
G/M = 2 L_c/D_c = 25
Total energy = 144 e.u.
u_{300} = 6.50 km/sec
u_{350} = 7.00 km/sec
(Run 24, Appendix A)

Reservoir conditions are taken at the throat entrance and are not necessarily maximum values

Figure 5. Calculated results for the 1-inch bore 72-gm model ballistic cycle.

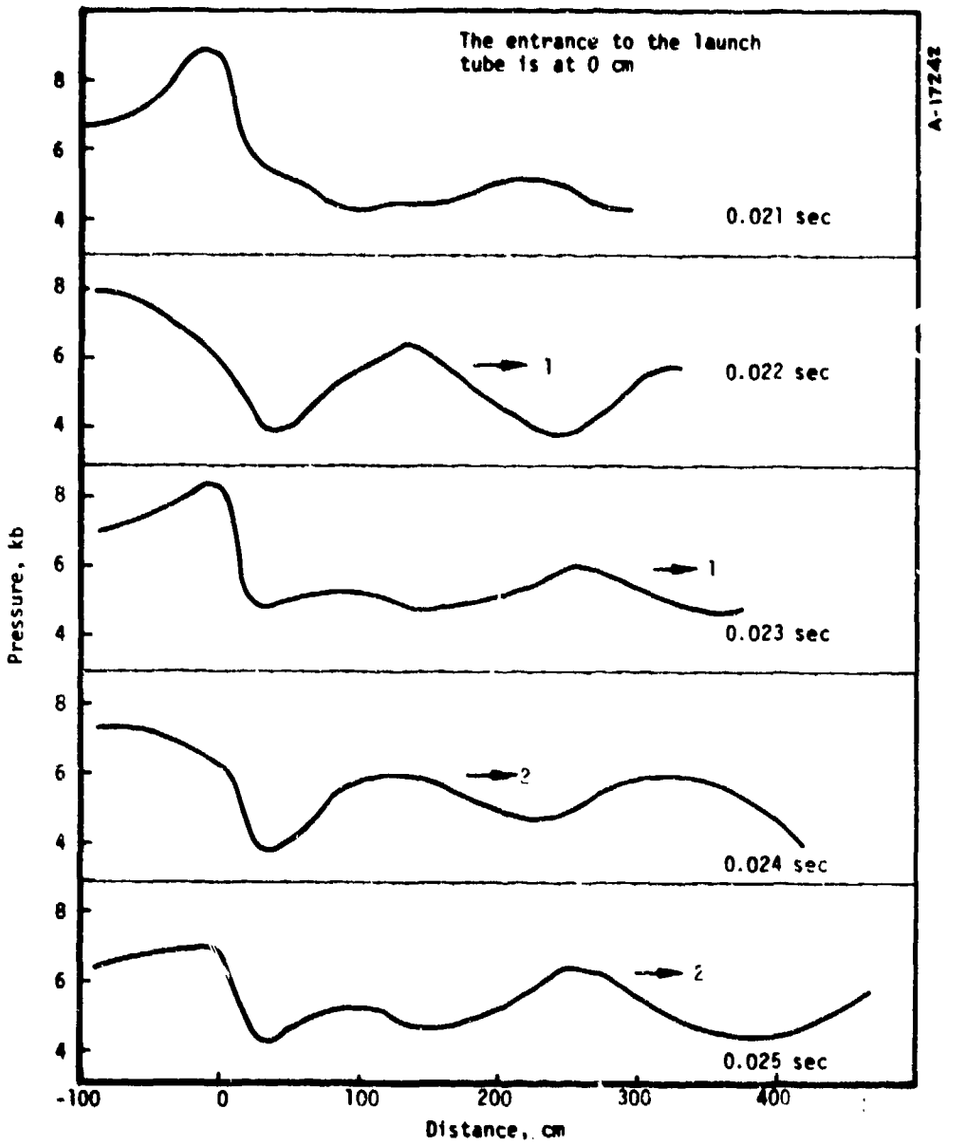

Pressure profiles from the face of the piston to the base of the model for the 1-inch bore 72-gm model launch cycle (Run 24, Appendix A)

Figure 6. Calculated pressure distributions during the hybrid launch cycle.

The effect of a more realistic initial gas distribution on the base pressure history is shown in Figure 7a. Here the injected gas is initially contained in the injection block and allowed to expand into the remainder of the compressor volume during the initial stages of compression. As a result, the first pressure pulse is enhanced and subsequent pulses reduced somewhat. Muzzle velocity is about 7 percent lower.

In most of the calculations, the model was unrestrained and because of its large areal density (ρl) did not suffer significant performance loss. The effect of a 2-kilobar shot-start condition was to increase the amplitude of the second base pressure pulse substantially as shown in Figure 7b and to increase muzzle velocity by only a few percent.

In this launch cycle, a zero shot-start condition appears most desirable and considerably simplifies the launch tube joint a the initial projectile location by eliminating the need for a diaphragm and by requiring only a thin shear disc on the base of the model.

2.4.3 112.5-gm Model, 1.25-inch Bore — Superbore Launch Cycle C

This launch cycle utilizes the same first stage, driver and compressor hardware as the previous two launch cycles but achieves substantially higher performance by using a larger bore launch tube and a saboted model. The "superbore" approach has many performance advantages but requires a sabot stripping operation after launch. This presents no difficulties in free-flight testing but would require considerable effort to accomplish for track-guided testing.

This cycle scales to a 12-pound, 4-inch diameter model after sabot stripping. The calculated launch velocity with a 300-caliber launch tube is 7.1 km/sec. The corresponding reservoir pressure and temperature histories and the model base pressure history are shown in Figure 8.

The calculated performance of 7.1 km/sec is well above the design performance of 6.1 km/sec and the cycle can be relaxed and still give a substantial performance margin.

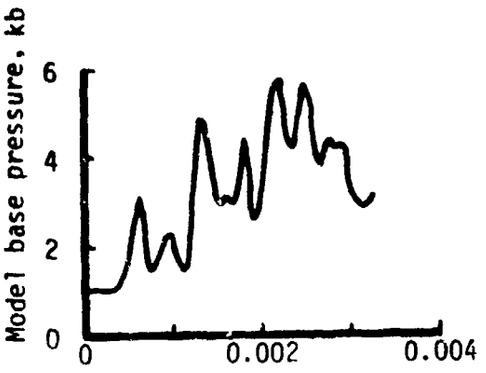

Even gas distribution
(Run 24, Appendix A)

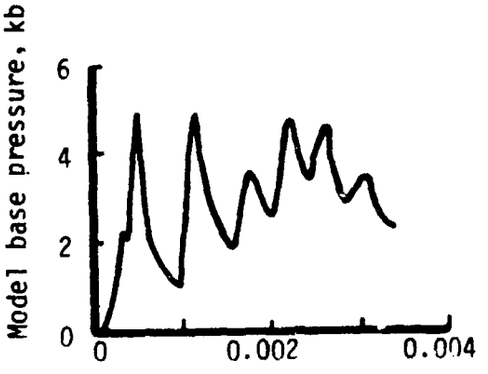

All gas initially in
injection block
(Run 26, Appendix A)

A-17247

a. 11.5-lb piston at 5000 fps
G/M = 2 L_C/D_C = 25
Total energy = 144

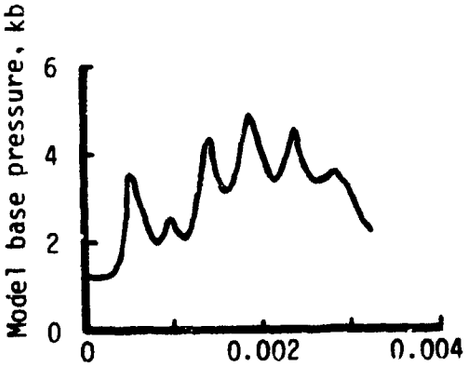

No shot start
(Run 16, Appendix A)

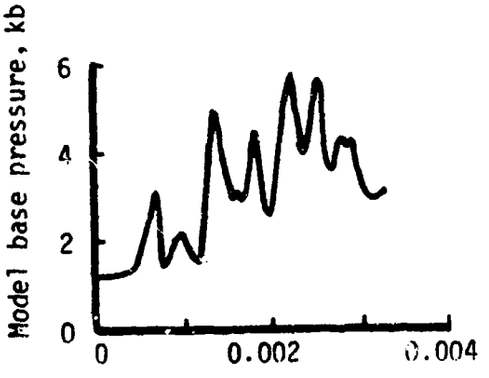

2-kb shot start
(Run 17, Appendix A)

b. 10.78-lb piston at 5000 fps
G/M = 2.4 L_C/D_C = 25
Total energy = 156 e.u.

Figure 7. Effect of initial gas distribution and shot-start condition on calculated model base pressure.

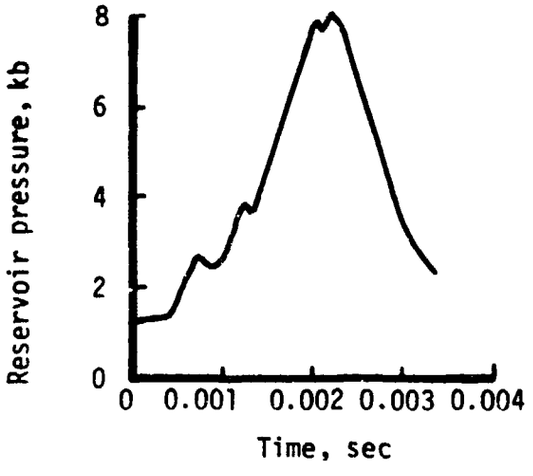

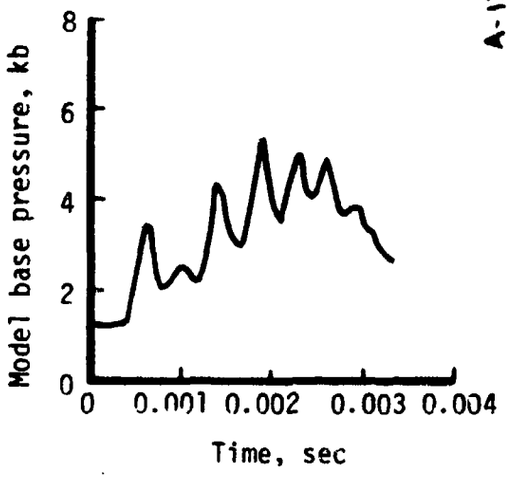

A-17252

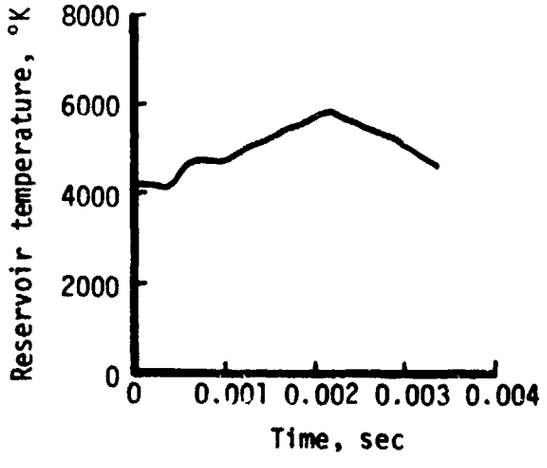

14 lbs piston at 5000 fps
G/M = 1.56 L_c/D_c = 25
Total energy =
u_{300} = 7.14 km/sec
u_{350} = 7.55 km/sec
(Run 39, Appendix A)

Reservoir conditions are taken at the throat entrance and are not necessarily maximum values

Figure 8. Calculated results for the 1.25-inch bore 112.5-gm model superbore ballistic cycle.

2.4.4 112.5-gm Model, 1.25-inch Bore — Relaxed Superbore Launch Cycle D

In this cycle, both the piston mass and velocity were reduced to relax peak reservoir conditions, primarily to reduce the heat loads on the interior walls of the launcher. Peak pressures of 7.3 kb and peak temperatures of 5600°K ease the design problems of both the reservoir pressure vessel and compressor throat and barrel liners as discussed later.

This relaxed cycle yields a calculated velocity of 6.6 km/sec after 300 calibers of travel. The corresponding reservoir pressure and temperature histories and the model base pressure history are shown in Figure 9.

The 112.5-gm superbore model assumes a 26.5-gm full length lexan sabot. If techniques can be developed to strip this sabot within a guided track, substantially higher-β models could be launched with the same first stage, driver and compressor hardware by increasing piston mass and velocity to generate maximum tolerable reservoir conditions.

2.4.5 Performance Sensitivity

The amount of gas injected into the compressor by the explosive drivers can be accurately determined through a series of driver tests, injection tests and calculational techniques as described later. Small variations in injected mass will arise as a result of the transient gas dynamics at injection, but final reservoir conditions and muzzle velocity are relatively insensitive to these as shown in Figure 10. However, if one of the four drivers fails to initiate, the loss of gas result in overcompression with the most probable consequence being local melting of the liner at the barrel inlet. The loss of two or more drivers could lead to pressure vessel failure.

The combination of injected gas mass and compressor volume at injection determine the compression isentrope. Since the injection gas mass can be accurately calibrated, the injection volume or piston position at injection can be used as an accurate control in choosing the compression isentrope. Piston energy at injection determines how far up the compression isentrope the cycle can proceed.

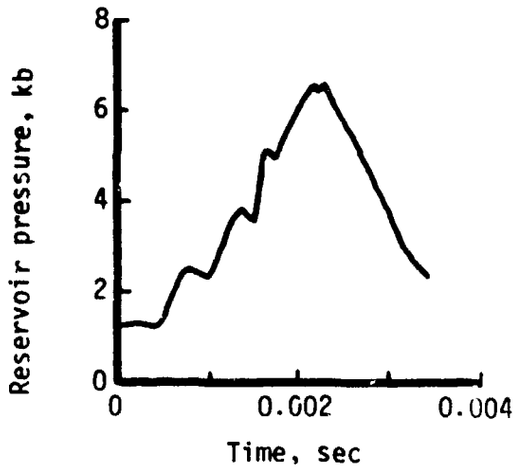

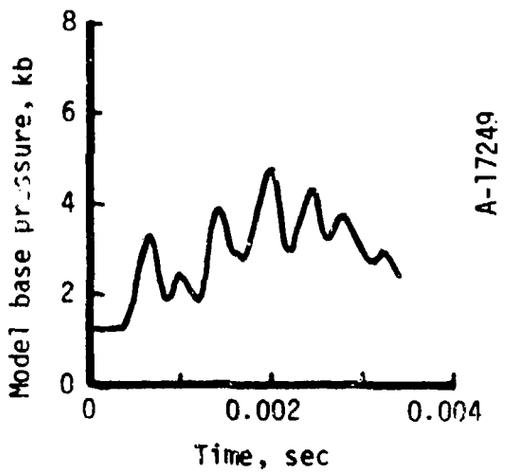

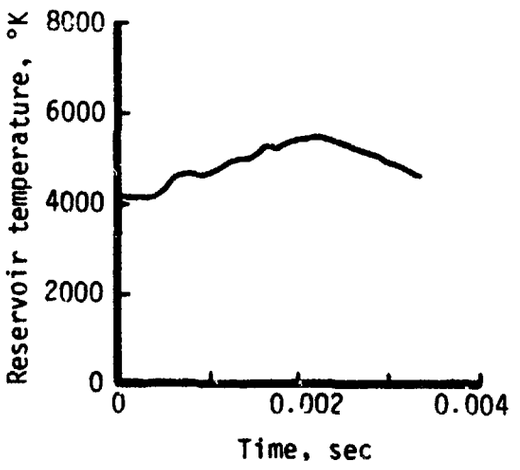

13-lb piston at fps
G/M = 1.56 L_c/D_c = 25
Total energy = 164 e.u.
u_{300} = 6.61 km/sec
u_{350} = 7.01 km/sec
(Run 37, Appendix A)

Reservoir conditions are taken at the throat entrance and are not necessarily maximum values

Figure 9. Calculated results for the 1.25-inch bore 112.5-gm model relaxed superbore ballistic cycle.

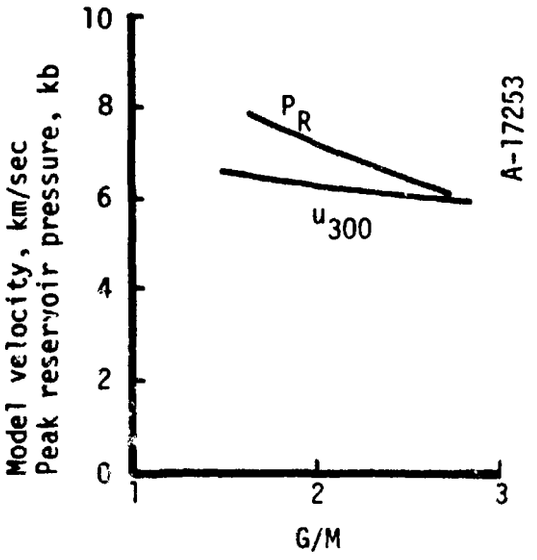

- 72-gram model
- 1-inch launch tube
- L_c/D_c = 25
- 10.78-lb piston at 5000 fps
- Injection gas energy density is 0.5764 e.u./gm

Injection gas mass to model mass ratio

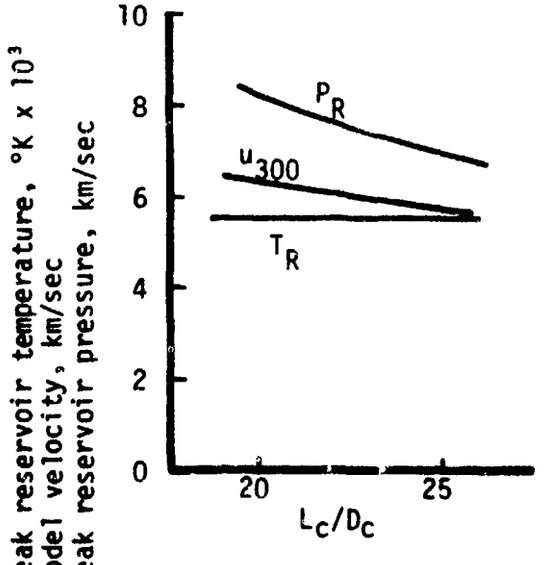

- 86-gram model
- 1-inch launch tube
- G/M = 2
- 10.78-lb piston at 5000 fps
- Injection gas energy density is 0.5764 e.u./gm

Injection piston position to compressor diameter ratio

Figure 10. Sensitivity of hybrid launcher performance to injection gas mass and piston position.

Piston mass/velocity characteristics (heavy/slow or light/fast) control the rate of progress up the compression isentrope. Thus, there is a great deal of independent control over the range of final reservoir states and the rate at which reservoir conditions are generated. Examples of performance variations with variable piston conditions are shown in Figure 11.

A small amount of hydrogen (typically less than 10 percent of the total gas mass) fills the compressor prior to injection. The amount of this "cold" gas can be used to fine-tune the injection energy density and can be used to help balance piston energy and mass/velocity characteristics with other parameters.

In practice, the above control parameters can be used separately or in combination to generate a ballistic cycle that optimizes performance and minimizes base pressure oscillations within the range of acceptable pressures and heat loads of the gun.

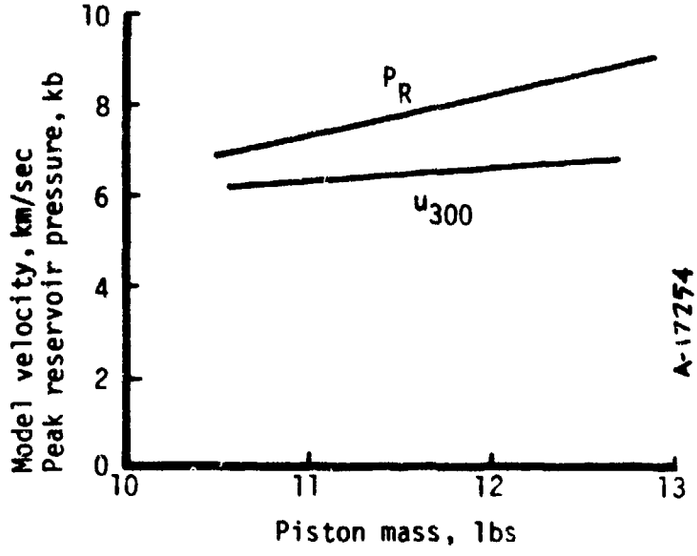

- 72-gram model
- 1-inch launch tube
- G/M = 2
- L_C/D_C = 25
- 5000 fps piston
- Injection gas energy density is 0.5764 e.u./gm

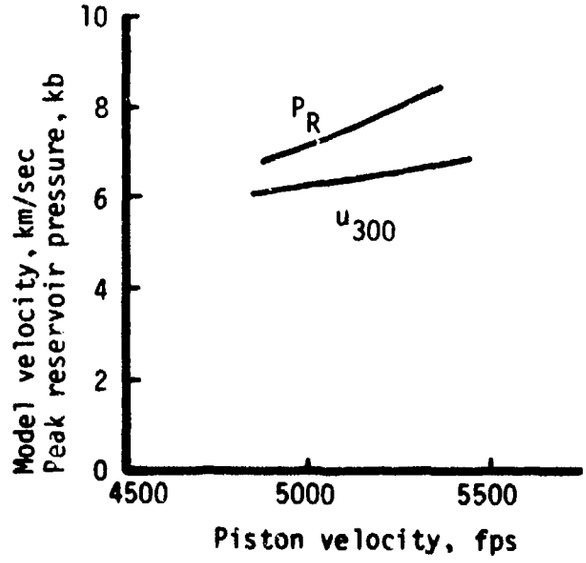

- 72-gram model
- 1-inch tube
- G/M = 2
- L_C/D_C = 25
- 10.78-lb piston
- Injection gas energy density is 0.5764 e.u./gm

Figure 11. Sensitivity of hybrid launcher performance to piston mass and velocity at injection.

SECTION 3

HEAT TRANSFER ANALYSIS AND LINER DESIGN

The analysis of Reference 2 concludes that energy losses due to heat transfer will not have a major effect on ballistic performance for a hybrid launch cycle using hydrogen. However, if heat transfer is severe enough to cause widespread melting of the gun interior, performance can be degraded. Even limited melting which will not penetrate the boundary layer in time to affect performance, will cause unacceptable damage to the compressor throat and launch tube. Thus, heat transfer limits performance in that it dictates the allowable conditions that will avoid melting the launcher components.

Using hydrogen, the dominating heat transfer mechanism is forced convection, which is controlled by the behavior of the gaseous boundary layer adjacent to the internal surfaces of the launcher components. Behavior of the boundary layer is complex in the extreme since it is subject to transient conditions in the region outside of the boundary layer, and transient thermal conditions on the wall side of the layer. Few analytical techniques exist for evaluating convective heat transfer behavior under conditions typical of guns. This design effort has made use of the approximate analysis technique that was developed in Reference 2.

3.1 PRELIMINARY ANALYSES

The results of Reference 2 show that a tungsten liner will melt in a 1-inch bore launcher when an 86-gm projectile is accelerated over 300 diameters to 6 km/sec while limiting the base pressure to 5 kilobars. In an effort to improve the heat sink capacity of tungsten, a composite of 0.25-mm tungsten backed up with copper was considered. It was hypothesized that the higher thermal diffusivity of copper would tend to draw the heat away from the heated tungsten surface and possibly eliminate the tungsten melt condition.

The selected thickness of tungsten is the minimum that will maintain the tungsten/copper interface below the copper melt temperature for the example considered. The analytical technique of Reference 2 is based on the results of a series of transient heat conduction solutions employing the CMA computer code (Reference 5) in conjunction with the boundary layer results for the 6-km/sec Simple Wave Launcher (SWL) cycle evaluated in Reference 2. Unfortunately, the maximum tungsten surface temperature is only reduced about 100°K due to the copper for the example evaluated. Consequently, this method of controlling the maximum tungsten temperature was abandoned.

Another method of protecting the launch tube from melting is to use an ablative liner. Calculations were performed, using the CMA code for the same conditions as above, employing graphite as the liner material. The ablation limits the graphite temperature to less than 2800°K. Maximum surface recession was calculated to be approximately 0.5 mm per launch cycle in a 1-inch bore launcher. This magnitude is sufficient to require liner replacement after each firing and could contaminate the flow to an extent that would degrade performance.

Based on these results, it seems that the launch requirements would have to be reduced and the ballistic cycle be carefully controlled in order to avoid replacement of liners after each launch. Consequently, more detailed studies were pursued with these thoughts in mind while retaining tungsten as the most promising candidate liner material.

3.2 DETAILED ANALYSIS OF BALLISTIC CYCLES

In principal, the basic boundary layer analysis technique of Reference 2 (and Reference 6 the predecessor to Reference 2) will apply to reasonably arbitrary inviscid boundary layer edge conditions. A significant limitation is that the technique will not do well under situations of inviscid flow reversals in time. Such flow reversals occur within the compressor and transition region to the launch tube during the ballistic cycle, and within the launch tube after the projectile exits the muzzle.

It is not possible within the budgetary limits of the present effort to extend the previous analysis to consider the departures of inviscid flow characteristics from those of the ideal cycles modeled in Reference 2 — the

Constant Base Pressure Launcher cycle (CBPL), and the SWL cycle mentioned previously. The current analysis makes use of (1) the inviscid properties obtained from the STEALTH 1-1/2-D calculations of the previous section; (2) the real hydrogen equation-of-state presented in Reference 2; (3) the CMA conduction solution methodology; and (4) correlations of results obtained from the CBPL and SWL boundary layer analysis procedures. The general procedure is presented below.

3.2.1 Heat Transfer Boundary Conditions

The heat transfer coefficient is given by:

$$H = \rho_i |u_i| C_h \tag{3}$$

where ρ_i and u_i come from the STEALTH ballistic cycle calculations, and C_h is the time and space dependent Stanton Number obtained from correlations of the CBPL and SWL boundary layer analyses. Note that Equation (3) allows consideration of flow reversals by using the absolute magnitude of velocity.

The wall heat flux is given by:

$$\dot{q}_w = H\left(h_i + \frac{u_i^2}{2} - h_w\right) \tag{4}$$

where $h_i = e_i + p_i/\rho_i$. The pressure, p_i, comes from the STEALTH output, and h_w comes from evaluation of the real hydrogen equation-of-state of Reference 2. The wall enthalpy is given by:

$$h_w = h_w(\rho_i, T_w, \text{hydrogen equation-of-state}) \tag{5}$$

and is shown in Figure 12.

The wall temperature is given by:

$$T_w = T_w\ (\dot{q}_w, \text{wall conduction solution}) \tag{6}$$

where $\dot{q}_w$ is evaluated from Equation (4) in conjunction with the mixed implicit/explicit finite difference conduction solution methodology of the CMA code, Reference 5.

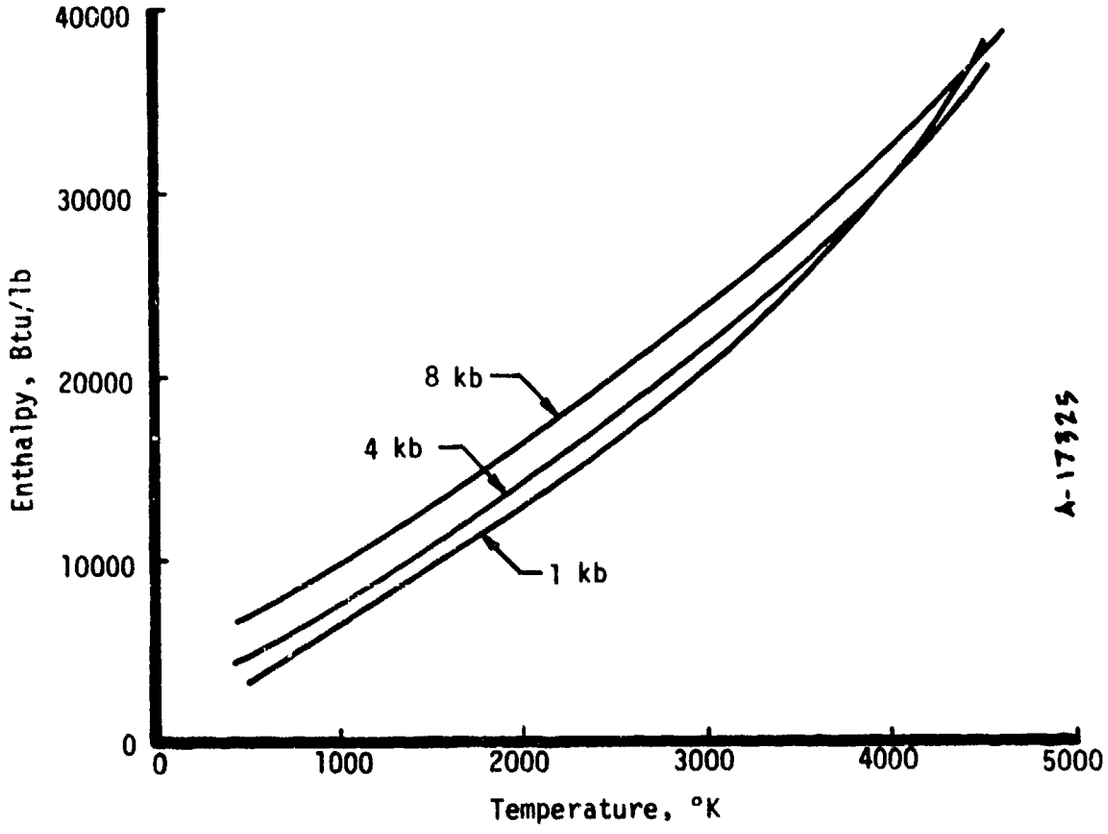

Figure 12. Wall enthalpy versus wall temperature for various pressures for the real hydrogen equation-of-state of Reference 2.

The C_h correlation is derived from CBPL and SWL results for a muzzle velocity of 6 km/sec. Figure 13 presents time and space variation of C_h from 1-inch and 5-inch bore launcher calculations. A reference curve is drawn through these results as a standard of comparison. Except for the short-lived spike that occurs when the base of the projectile passes a given axial position, the Stanton numbers do not depart from the reference curve by more than 35 percent. Thus, the reference curve serves as a fair representation of the results for diverse boundary conditions and launcher sizes.

Figure 14 presents the correlation that has been employed for the present analysis for all launcher sizes and all times during the ballistic cycle. It is different from the reference curve due to adjustments based on experience to account for the following factors:

- The CBPL and SWL Stanton numbers are based on the solution of the momentum boundary layer and application of Reynolds analogy. The Chilton-Colburn analogy (Reference 7) dictates higher Stanton numbers for Prandtl number less than unity such as for hydrogen. This dictates an upward adjustment from the reference curve.
- The wall shear correlations of References 2 and 6 yields lower friction factors than are experienced at high Reynolds numbers on momentum thickness, Re_θ, also dictating an upward adjustment of the reference curve
- Higher friction factors yield higher values of Re_θ which dictates a downward adjustment from previous adjustments
- The analysis of Reference 2 evaluates wall shear at the wall temperature ratio, T_w/T_i, of 0.2. For most of the time, wall temperature ratio is considerably higher than 0.2. This also dictates a downward adjustment from previous adjustments.
- The CBPL and SWL analyses assume zero boundary layer thicknesses at the chambrage plane, which yields infinite heat transfer coefficients. The actual finite thicknesses of boundary layers here prompts a significant downward adjustment of the results at and near the chambrage plane.

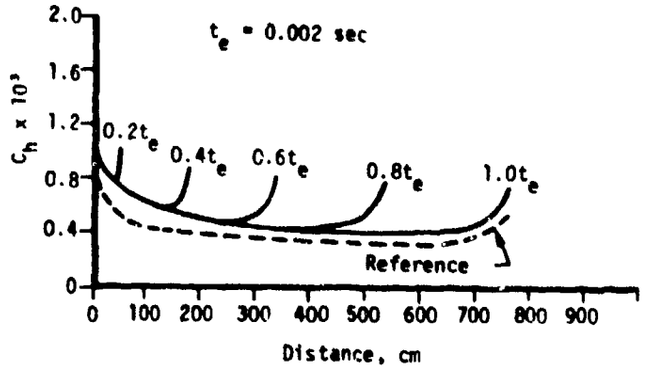

a. Simple wave launch cycle 1-inch launch tube

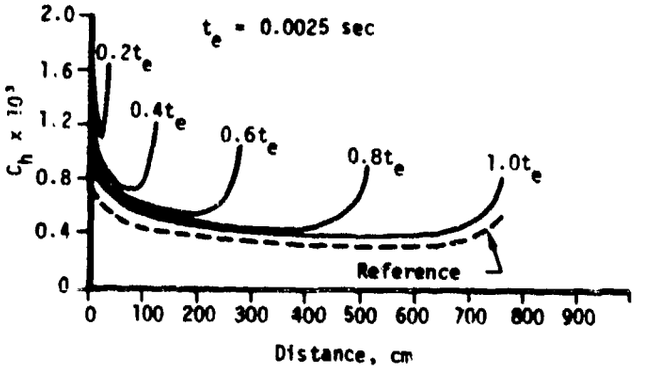

A-17326

b. Constant base pressure launch cycle 1-inch launch tube

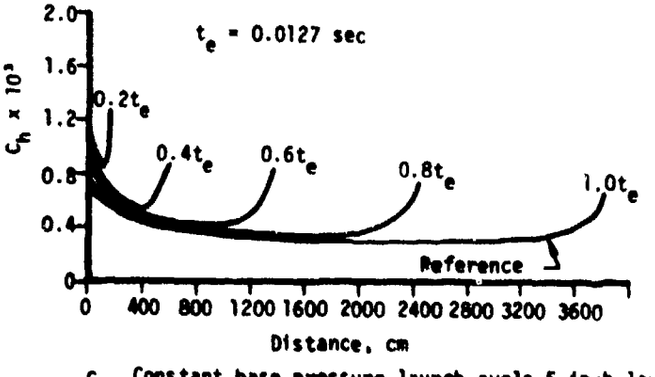

c. Constant base pressure launch cycle 5-inch launch tube (superbore)

Figure 13. Temporal and spatial variation of Stanton number, C_h, for various ballistic cycles.

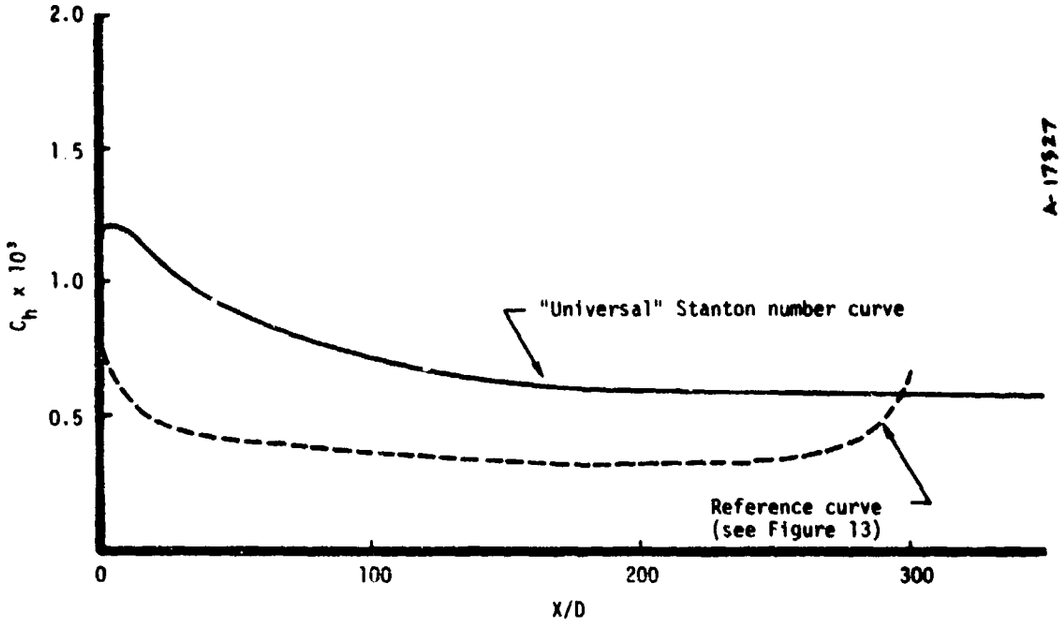

Figure 14. Stanton number, C_h, distribution in the launch tube for all times, for all launcher sizes and all ballistic cycles.

3.2.2 Results with Tungsten Liners

The heat transfer analyses went hand-in-hand with the ballistic analyses discussed in Section 2. This was dictated by the requirement to design a system which not only performed ballistically but survived the ballistic cycle without melting both in subscale and full scale. Because of the longer exposure times, heat transfer problems are expected to be more severe in full scale.

The preliminary analyses together with the results of Reference 2, suggested that melting would occur in subscale and full scale under the conditions of Ballistic Cycle A. Thus, Cycle B was evolved to relax the heat transfer environment. Calculations were performed for this cycle at the chambrage plane employing the heat transfer parameters described above. The appropriate inputs of chambrage plane pressure, total enthalpy, and heat transfer coefficient are presented in Figure 15 along with the computed wall temperature response.

Maximum surface temperature is 3560°K. This is 83°K below the melt temperature of tungsten of 3643°K reported in Reference 8 (other sources report melt temperatures from 10 to 60°K higher than that of Reference 8). In-depth temperature profiles from the calculation are shown in Figure 15, showing maximum temperature gradients of about 1.2×10^5 °K/cm and showing the narrowness of the effected region in the material during the ballistic event (only about 0.04 cm of tungsten is above 1000°K when the projectile travel is 300 calibers, t = 0.003 sec). It is notable that the peak surface temperature nearly coincides with the peak total enthalpy, pressure, and heat transfer coefficient. This suggests that even though tungsten is a good heat sink material, it still acts somewhat like an insulator when subjected to the very large maximum heat flux of about 1.3×10^6 Btu/ft^2-sec.

Ballistic Cycle B in full scale causes melting (T_{max} = 3851°K) at the chambrage plane. In an effort to mitigate the full-scale heat transfer problem while increasing model weight, the superbore concept was evaluated, both ballistically and in terms of heat transfer. Ballistic Cycle C is overdesigned relative to ballistic performance, and its heat transfer behavior was not evaluated. However, Ballistic Cycle D accomplishes the ballistic

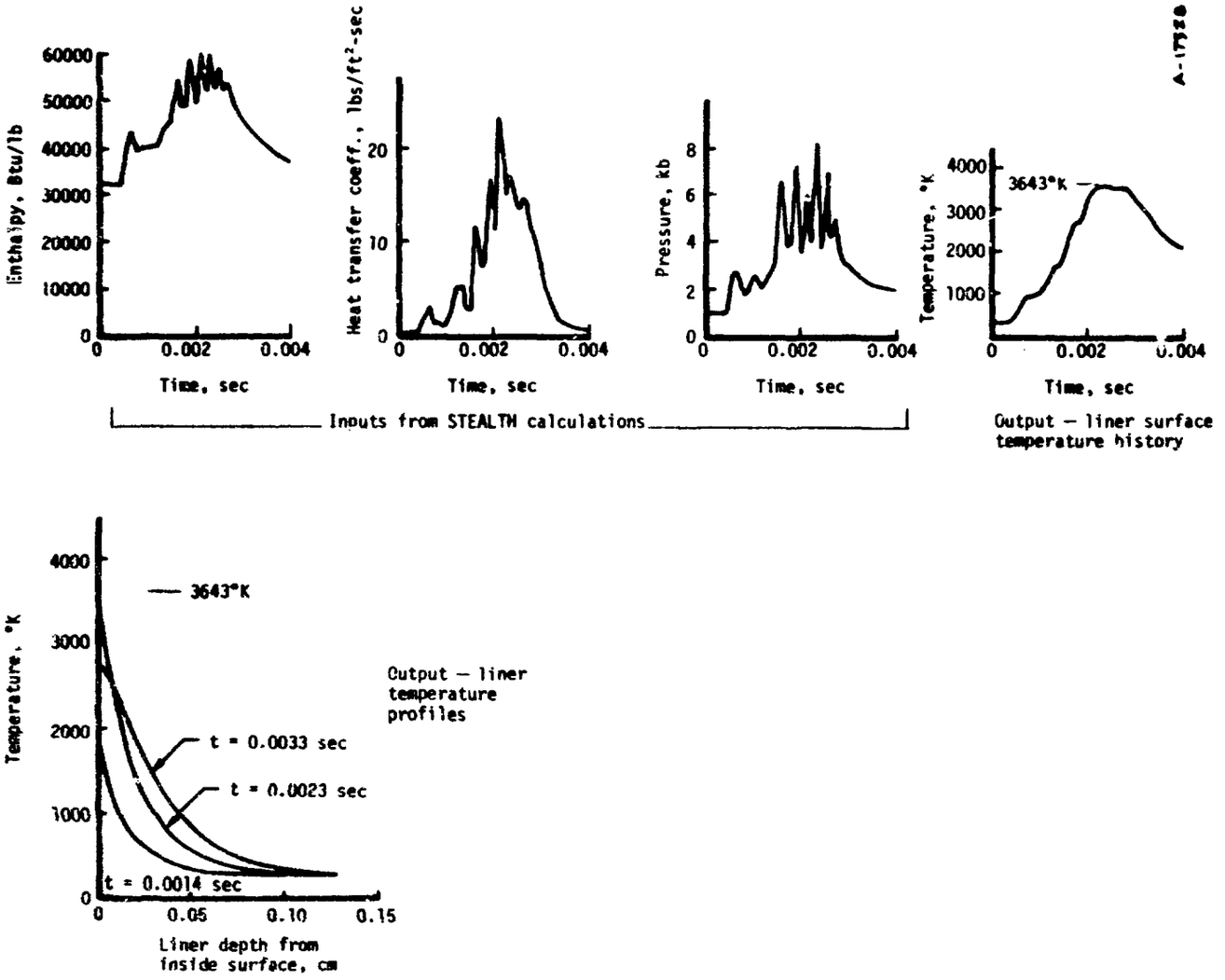

Figure 15. Heat transfer calculations for 1/4-scale launcher Cycle B with a tungsten liner.

objectives with sufficient margin but under more relaxed reservoir conditions. The heat transfer analysis of the full-scale ballistic cycle predicted a maximum temperature approximately 75° below the tungsten wall melt temperature. Subscale temperatures, of course, would be lower.

The maximum temperature results for the various cycles and the times when they occur are summarized in Table 2.

TABLE 2. MAXIMUM TEMPERATURES (°K) AND TIMES (SEC) OF PEAK TEMPERATURE FOR DESIGN BALLISTIC CYCLES, TUNGSTEN T_{MELT} = 3643°K

Cycle	Subscale	Full Scale
A	—	—
B	3560/0.023	3651/0.084
C	—	—
D	—	3565/0.089

The acceptable cycles ballistically and in terms of avoiding melting are Cycle B in subscale, and Cycle D, both in subscale and full scale. However, none of these cases have much margin. The desired margin is obtained by overlaying the tungsten with a thin layer of a material with a higher melt temperature than tungsten.

3.2.3 Composite Liner Performance

Tantalum carbide heat sink properties yield exposure times to melt only approximately half as large as tungsten. However, it has a higher melt temperature (4153°K, Reference 8) and is a good material to vapor deposit on tungsten (Reference 9). It was theorized that the temperature response of a thin layer of tantalum carbide over tungsten would be governed more by the heat sink properties of tungsten than by the properties of the tantalum carbide. On the other hand, the "insulative" properties of a thin

layer of tantalum carbide should protect the tungsten from experiencing such high temperatures. The expected sacrifice was a slight increase in the maximum bore surface temperature, depending on the thickness of the layer. Tantalum carbide is more brittle than tungsten, but it is harder and probably has better wear resistance.

Figure 16 presents the chambrage plane surface and interface temperature responses for a tungsten, tantalum carbide composite for Cycle B in subscale, as well as the tungsten results of Figure 15. The composite consists of 0.005 cm of tantalum carbide over 0.064-cm tungsten which is deposited inside the steel barrel of the launcher, or a steel liner. Early in the cycle, the tantalum carbide layer increases the surface temperature over that experienced by tungsten without the layer. Later in the cycle, the tungsten surface temperature without the layer slightly exceeds the surface temperature with the layer. However, the maximum tungsten temperature in the composite is reduced to about 2610°K, a comfortable margin of about 1000°K below the tungsten melt temperature. The tantalum carbide maximum temperature is 3875°K, approximately 280°K below its melt temperature. The maximum temperature of the steel occurs approximately 0.003 sec after the projectile passes 300 calibers.* The steel is clearly below its melt temperature by about 1000°K.

The full-scale heat transfer performance of Cycle B with the same composite is shown in Figure 17. Results are similar to the subscale version, except all maximum temperatures are higher. Note that Cycle B is now feasible in full scale, with all materials being maintained below their melt temperatures. A somewhat thicker tungsten layer might be desirable in full scale to depress further the maximum temperature of the steel substrate.

Some experience exists using vapor-deposited tungsten to improve gun barrel performance (Reference 9). Cracking is expected to occur in the tungsten to form "tiles." However, it is considered opinion that cracks are

*Fluidynamic behavior at the chambrage plane after the projectile passes 300 calibers is modeled herein by allowing the projectile to continue to accelerate in the barrel and evaluating the late term STEALTH output.

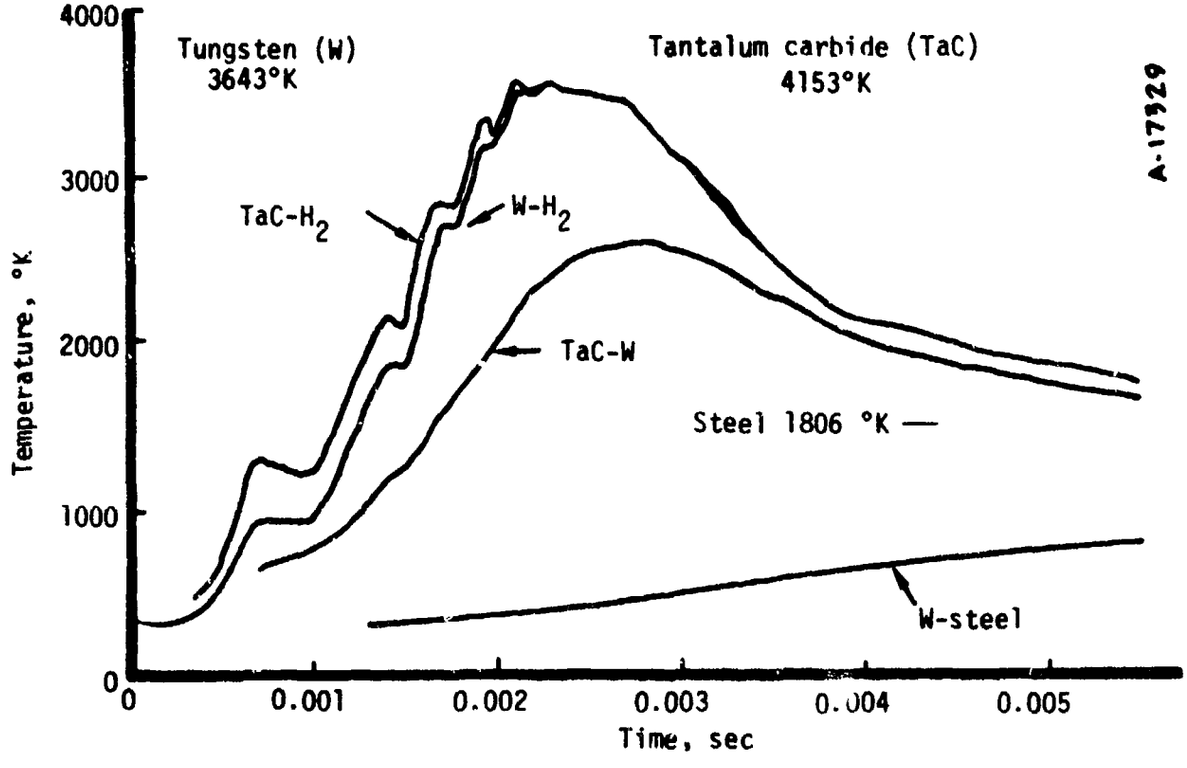

Temperature histories at the barrel inlet of a 1-inch bore hybrid launcher with a 72-gm model (Cycle B)

Figure 16. Calculated temperature histories for a tungsten liner and a composite liner in the 1/4-scale launcher.

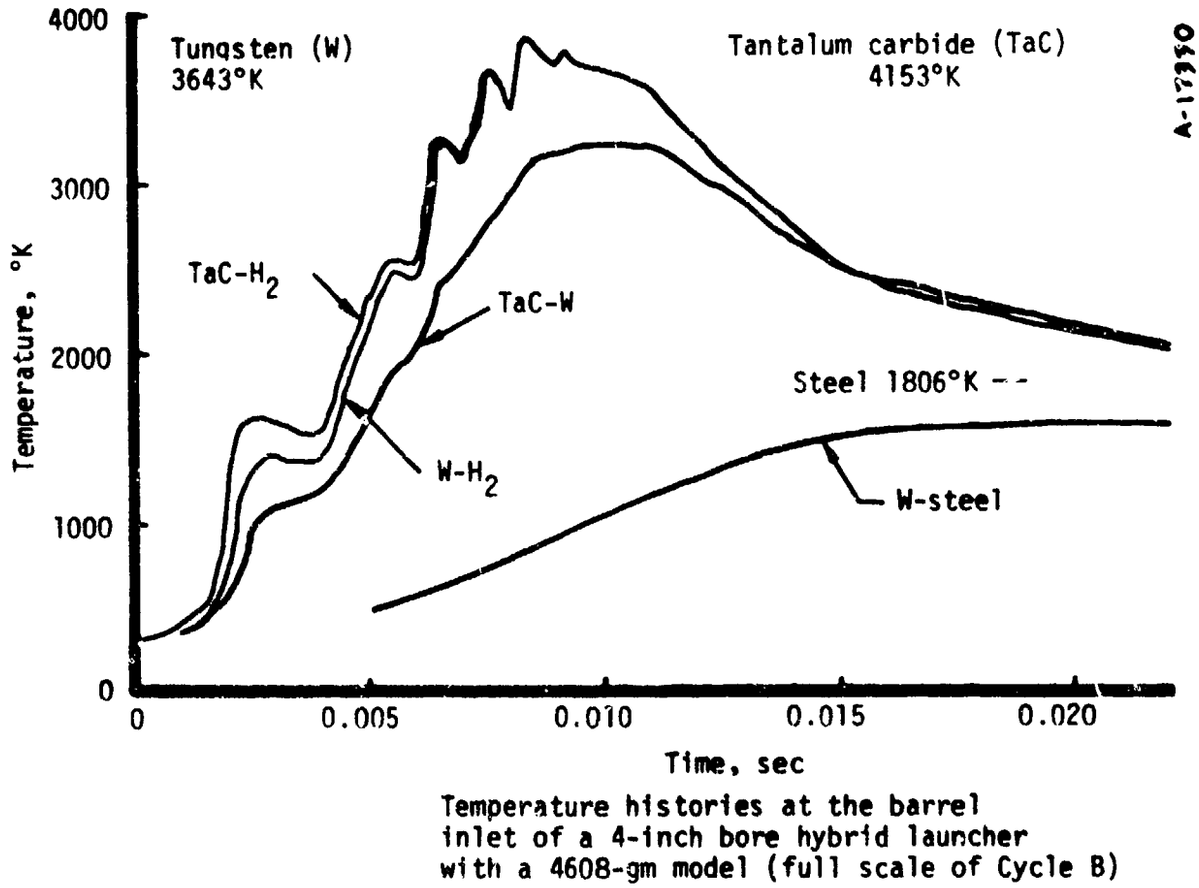

Figure 17. Calculated temperature histories for a tungsten liner and a composite liner in the full-scale launcher.

not intrinsically harmful, providing good bonding exists between the tungsten and the steel. The thinness of the tantalum carbide suggests that it will follow the behavior of the tungsten, cracking where it cracks, with possibly additional submicroscopic cracks.

The composite liner performance downstream of the chambrage plane has been evaluated for Cycle B in subscale. The results in Figure 18 show that peak surface temperatures are reduced only slightly with later exposure at the higher L/D's. For example, at an L/D of 200, maximum surface temperature is only 700°K below the maximum at the chambrage plane. Based on these results, the subscale launcher design incorporates a liner along the entire length of the launch tube.

The boundary layer analysis upon which the heat transfer coefficients are based is only approximate. To evaluate the sensitivity of the heat transfer analysis to these approximations, the heat transfer coefficient at the chambrage plane for subscale Cycle B was doubled. As a result, the maximum computed tantalum carbide surface temperature was increased to 3831°K and the tungsten interface temperature was increased to 2736°K. Although this lowers the margin to melt somewhat, it gives confidence that the approximations used in the boundary layer analysis are reasonable.

Average heat transfer coefficients upstream of the throat in the compressor section should be much lower than at the chambrage plane, by at least an order of magnitude (the compressor cross section here is 16 times larger than at the chambrage plane, leading to very much lower boundary layer edge mass fluxes). Transient heat transfer calculations were performed for the compressor section with the compressor steel exposed to the hydrogen. Heat transfer input was the same as used at the chambrage plane except that heat transfer coefficients were reduced by a factor of 10. Maximum computed steel temperature is 1778°K, suggesting that the compressor section does not need to be protected with a liner.

Thus, the subscale launcher thermal protection system will consist of composite liners in the convergent throat section and launch tube. Plated surfaces with the same composition as the liner will also be incorporated opposite the drivers to protect the compressor from the high heat fluxes experienced during injection.

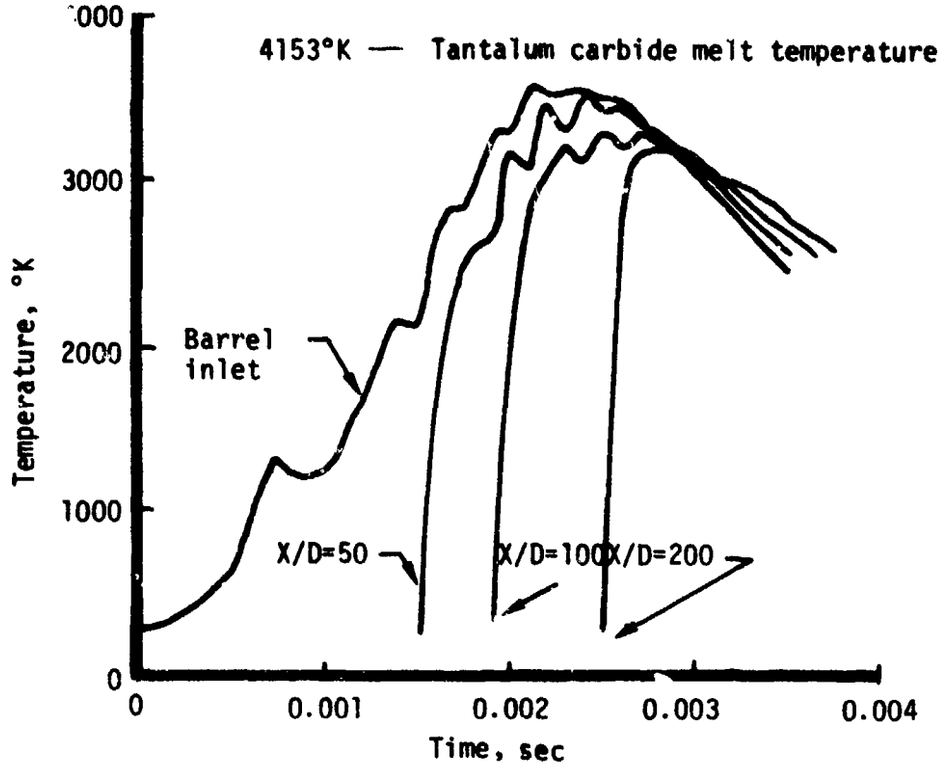

a. Liner surface temperature histories

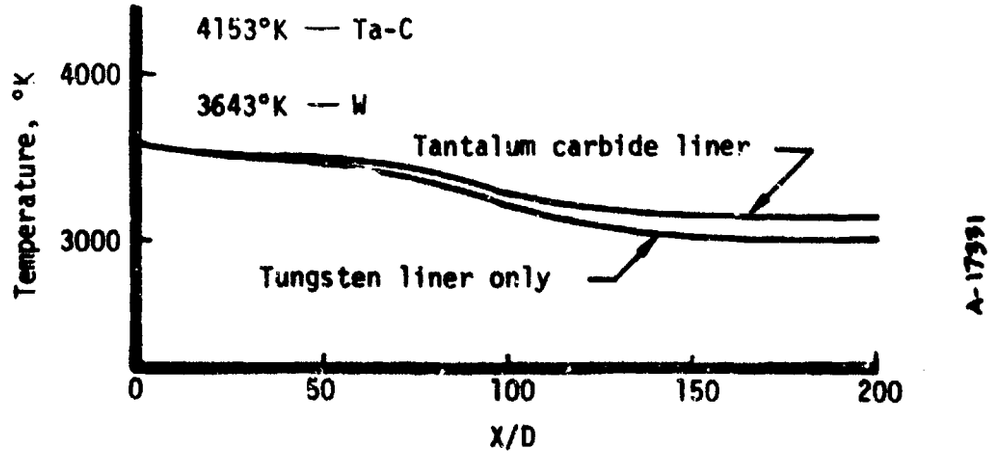

b. Peak liner surface temperatures along the launch tube

Figure 18. Surface temperatures along the launch tube for the 72-gm 1-inch diameter projectile — Cycle B.

SECTION 4

EXPLOSIVE DRIVER DESIGN

The explosive driver is a device used to convert the chemical energy of an explosive through a progressively collapsing metal tube to the internal and kinetic energy of the driver gas. The operation of a typical explosive driver is shown schematically in Figure 19. The range of performance and operational characteristics of these devices has been reported by several investigators (References 10 and 11).

Several explosive drivers are used by the hybrid two-stage gun to inject high energy gas into the compressor section. As a result, a substantially extended range of high pressure, high temperature compression states are possible for the two-stage ballistic cycle with corresponding increases in launch mass capability.

4.1 INJECTION OF DRIVER GAS

In previous attempts to develop a hybrid two-stage gun (Reference 1), injection gas losses were one of the major causes of poor performance. Two factors contributed to these losses. First, the large driver-to-compressor area ratio resulted in choked flow and reduced injection rates. Second, a substantial fraction of the gas was trapped between the injection ports and explosive driver terminations by the passage of the piston.

In the present design, the injection process shown schematically in Figure 20 was simplified by using several small drivers appropriately spaced along the injection block.

The driver-to-compressor area ratio is kept sufficiently low that choking problems are avoided. The drivers inject normal to the compressor

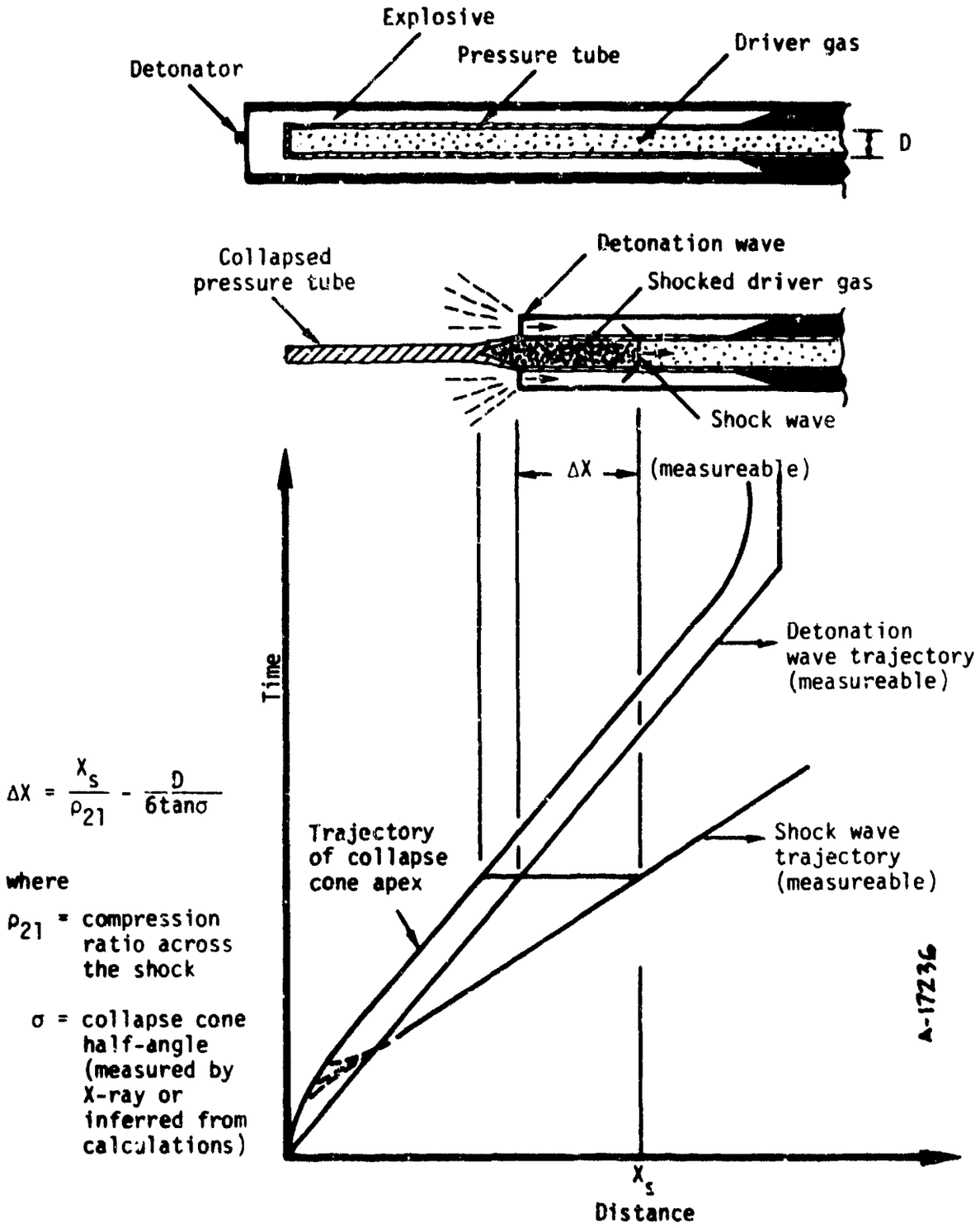

$$\Delta X = \frac{X_s}{\rho_{21}} - \frac{D}{6\tan\sigma}$$

where

ρ_{21} = compression ratio across the shock

σ = collapse cone half-angle (measured by X-ray or inferred from calculations)

Figure 19. Schematic of explosive driver operation.

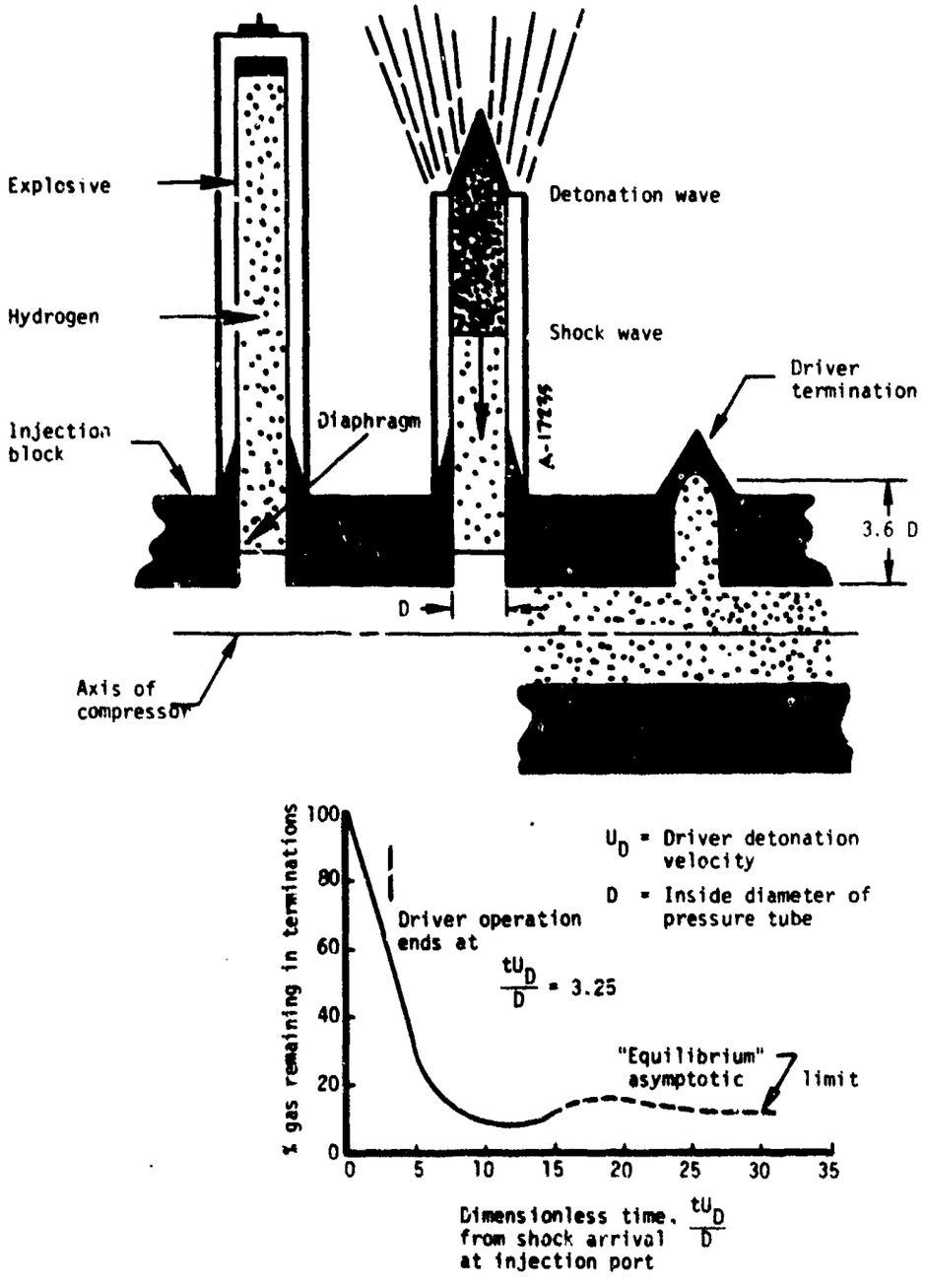

Figure 20. Schematic of injection process and calculated mass injection rate.

axis and the gas can, in effect, expand in both directions into the compressor. This is equivalent to about a 7:1 area expansion which is sufficiently large to prevent choking.

The driver termination was placed as close as practically possible to the injection port to minimize the amount of gas trapped when the piston closes off the injection port. Specifically, the termination is 3.6 pressure tube diameters from the injection port.

The STEALTH 1-1/2-D Lagrangian code described previously was used to estimate the fraction of driver gas that would be trapped between driver termination and injection port. The results of these calculations are shown in Figure 20 where it can be seen that 8 to 16 percent of the driver gas can be trapped depending on the timing of port closure. Most likely closure will be delayed so the "equilibrium" gas losses will apply. To this must be added some margin for leakage through an imperfectly formed driver termination. For design purposes, 16 percent of the driver gas is assumed to be lost at injection. The actual loss fraction will be determined experimentally in driver and injection tests which will be designed to accurately measure the mass of gas delivered during injection.

4.2 DRIVER DESIGN CONSIDERATIONS

In designing the ballistic cycle for the hybrid two-stage gun, the contribution to the energy of the gas by the drivers and the piston must be carefully balanced. An injection energy density of about 0.575 eu/gm (see Figure 1) was found to be most suitable. This is very close to the energy density that would be delivered by drivers using nitromethane explosive in an arrangement where all the gas is processed by the explosive drivers. On the other hand, certain cost and hardware advantages could be realized with drivers using Octol explosive which, because of its higher detonation velocity, can deliver gas at a much higher energy density.* At this energy density

*Nitromethane has a nominal detonation velocity of 6.3 km/sec and injects gas at an energy density of ~0.58 eu/gm. Octol has a detonation velocity of 8.48 km/sec and injects gas at an energy density of ~0.86 eu/gm.

level on the proper compression isentrope to give maximum tolerable reservoir pressures and temperatures (Figure 1), there is, however, little room for control of reservoir conditions by the piston. In fact, the model base pressure limit of 5 kilobars has already been exceeded. A better balance between driver and piston energy is required to independently control final reservoir state and rate of reservoir buildup so as to approach a constant base pressure launch cycle. To reduce the energy density at injection to a more workable level, the gas injected by the Octol drivers would have to be mixed with "cold" gas initially in the compressor.

In practice, drivers using Octol explosive would inject about 60 percent of the total gas into the system. Proper performance then depends critically on the complete mixing of the "hot" driver gas with the "cold" compressor gas. A ballistic cycle calculation was carried out for the worst case in which the hot gas pushed the cold gas with no mixing; the result was the performance of a cold gas gun with the heat transfer problems of a very hot gas gun.

The complete mixing of 60-percent hot gas with 40-percent cold gas was considered too uncertain and likely to result in erratic, poor performance. Consequently, the decision was made to use nitromethane drivers in the present hybrid launcher design. Using nitromethane, 92.5 percent of the total gas would be delivered by the explosive drivers. The other 7.5 percent would be cold gas initially in the compressor. With this ratio of hot to cold gas, complete mixing can be expected. Furthermore, as described previously, the small amount of cold gas initially in the compressor can be varied to fine-tune the equilibrium energy density at injection.

The nitromethane driver shocked gas conditions were computed using the real hydrogen equation-of-state and the full shock Hugoniot relations (Reference 2). These conditions are summarized in Table 3. The 6.5-kilobar shocked gas column precompresses the nitromethane explosive causing the detonation velocity to increase. This effect is accounted for in Table 3 since it has an important role in determining final driver gas energy.

TABLE 3. GASDYNAMIC PARAMETERS FOR THE EXPLOSIVE DRIVERS USED IN THE HYBRID LAUNCHER

(All values based on the real hydrogen equation-of-state of Appendix A, Reference 2)

Loading Density	0.01 gm/cm^3
Loading Pressure at 20°C	1982 psia
Shocked Gas Pressure	6.5 kb
Shocked Gas Velocity (also the detonation velocity of a 6.5-kb nitromethane driver)	6.82 km/sec
Shocked Gas Density	0.037 gm/cm^3
Compression Ratio Across the Shock	3.7
Shock Velocity	9.35 km/sec
Shocked Gas Temperature	2483°K

4.3 EXPLOSIVE DRIVER DESIGN

The design of the nitromethane explosive drivers takes into account the following phenomena:

- Driver startup losses
- Radial expansion
- Jetting
- Premature explosive decomposition
- Driver termination

There is a metal plug in the upstream end of the pressure tube which interferes with the initial collapse process and causes some gas to be lost during piston formation. Based on data from a well-tested 6.5-kilobar nitromethane driver (Reference 11), the gas initially in the first 2 diameters of the pressure tube is lost during driver startup. This loss is taken into account in determining the proper length of driver to deliver the required mass of gas.

A properly operating explosive driver can be characterized by a number of parameters involving diameters, wall ratios and mass ratios. These are summarized in Table 4 for the driver of Reference 11 and the current design.

The design represented by this set of parameters is then evaluated by a combined Lagrangian expansion — collapse calculation. Maximum driver expansion occurs at the beginning of the driver termination where the time between shock arrival and detonation arrival is longest. Pressure tube expansions of up to 30 percent can be tolerated without adversely affecting driver performance (Reference 11). The rate of expansion is primarily controlled by the inertia of the pressure tube, explosive, and tamper, while material strengths play a secondary role. The expansion phase of driver operation is modeled quite accurately by this calculational technique (Reference 11).

When the time of maximum expansion is reached in the calculation, the equation-of-state of the explosive region is switched from an inert liquid to an explosive products description. The pressure tube motion is reversed and

TABLE 4. SUMMARY OF EXPLOSIVE DRIVER DESIGN PARAMETERS

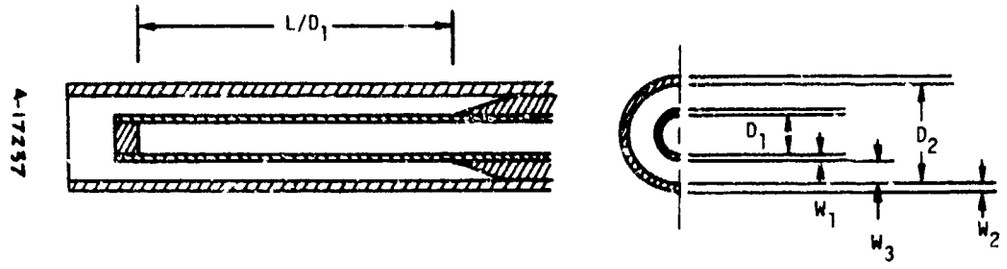

Driver Design	Operating Pressure (kb)	L/D_1	C/M	w_1/D_1	w_2/D_2	w_3/D_1	Maximum Pressure Tube Expansion
Hybrid Launcher	6.5	34[a]	1.63	0.0531	0.129	0.415	29%[a]
Alpha-1 Ref. 11	6.5	27	1.82	0.0469	0.153	0.414	20%

[a]Applicable to the drivers used in the superbore launch cycle. The drivers used for the 72-gm model launch cycle would have an L/D_1 = 28 and a maximum expansion of 27 percent.

collapse takes place. This one-dimensional calculational technique should not be relied upon, however, to predict pressure tube collapse since the actual collapse process is two-dimensional. In practice the one-dimensional collapse calculations are used as a guide and driver parameters that ensure proper collapse characteristics are determined ultimately by experiment.

On the basis of a large number of driver parametric tests, jetting of high pressure nitromethane drivers is not observed except for very large C/M ratios. For example, drivers operating in the 4- to 8-kilobar range exhibit near-ideal performance over a considerable range of C/M ratios and are not sensitive to modest variations in the C/M ratio.

When high pressure drivers are scaled up, the possibility of premature explosive decomposition must be considered. As shown in Figure 21, the driver shock propogates into the explosive ahead of the detonation wave. For a 6.5-kilobar driver, pressures on the order of 10 kilobars can be developed in the explosive as a result of shock reflection. Given enough time, the explosive will release a significant amount of energy as decomposition proceeds around adiabatically compressed bubbles (Reference 11). For a 9-inch driver such as currently proposed for the full-scale hybrid launcher, the explosive exposure times are long enough that premature decomposition can be well developed. This can be reduced to a negligible effect by prepressuring the explosive to a few hundred psi (Reference 11).

The driver termination plays a critical role in the operation of the hybrid launcher since it must form an effective seal preventing the leakage of high pressure, high temperature hydrogen until the injection ports are closed off by the piston. It is the critical interface between the explosive drivers and the two-stage gun. Design of the driver termination is based largely on experience with past designs. Taper angles (see Figure 23) of between 5° and 10° have been used in the past for successful closures. The final design for the driver termination will be evolved as part of the driver development tests and injection tests and will be based on the best combination of reliable performance and low replacement costs.

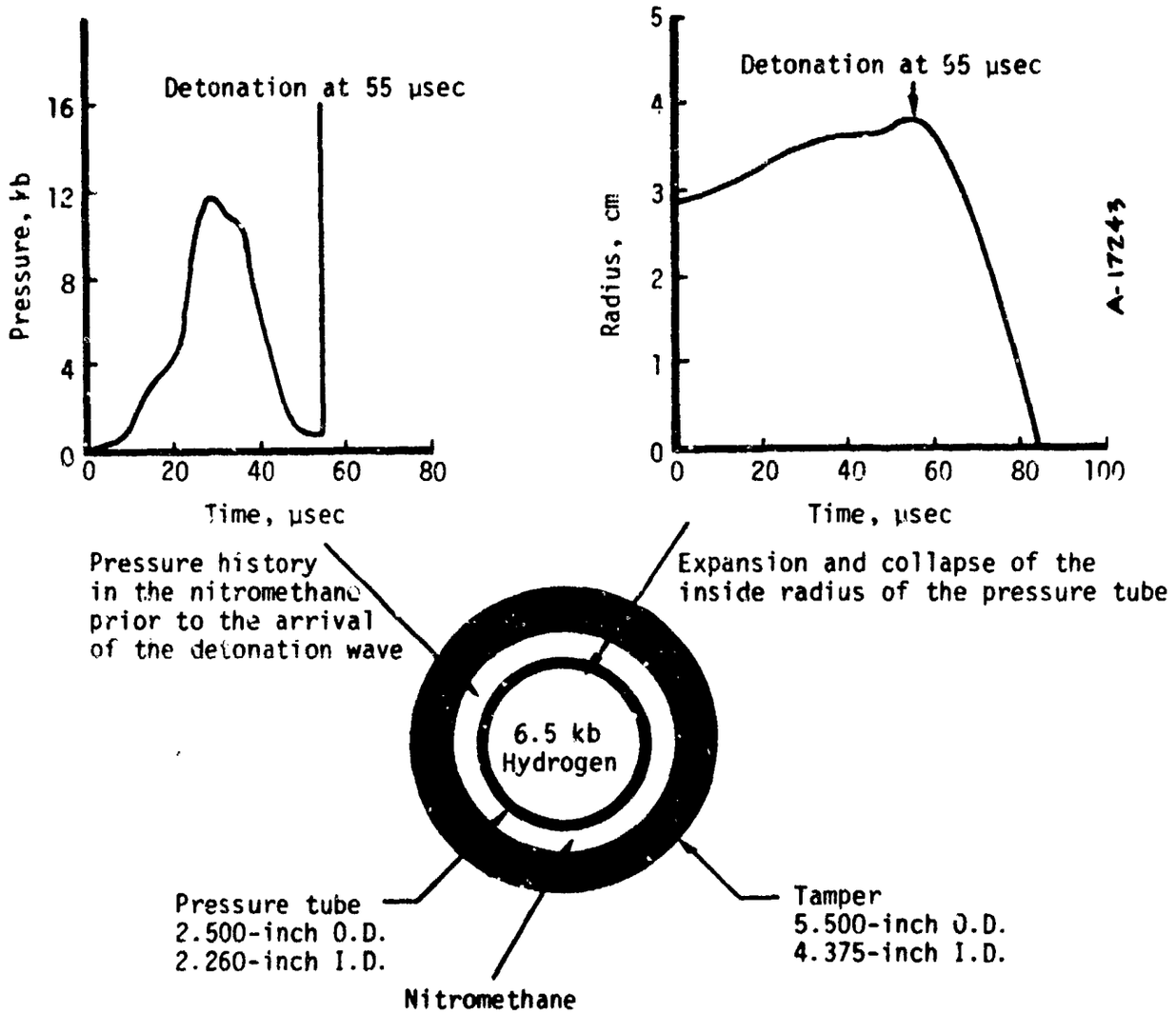

Figure 21. Calculated characteristics of the explosive driver for the 1/4-scale hybrid launcher.

SECTION 5

SYSTEM DESIGN

The ballistic cycle design and thermal protection techniques will first be tested in 1/4 scale. A modified 105-mm gun will be used as the first stage to drive a 1- or 1-1/4-inch bore launch tube. The hardware design described in this section is specific to the 1/4-scale tests and is not intended to be scaled directly to full scale. The primary objective of the 1/4-scale design is to demonstrate the ballistic cycle performance limits and thermal protection strategies developed in the design analysis. Once these are established, the design of the full-scale launcher hardware will be initiated. The full-scale design will incorporate, for example, a more efficient explosive driver design, an optimized compressor section pressure vessel design and a thermal liner design for rapid installation and removal.

5.1 OVERALL SYSTEM

The overall design of the 1/4-scale hybrid launcher is shown in Figure 22. The first stage consists of a smooth bored M68 105-mm high-performance tank gun with a 25-caliber barrel extension. The first stage piston will be a solid polyethylene cylinder with obturator.

Four explosive drivers spaced along the injection block will be preloaded with about 2000 psia hydrogen. Each driver will contain about 50 grams of gas which includes allowances for losses. The first stage and compressor section will be loaded initially with about 25-psia hydrogen (~14 grams) contained between the piston face and model base. Thin stainless steel diaphragms will separate the driver gas from the compressor gas.

The compressor section consists of three parts: the main unlined pressure vessel, the thermally-lined throat and barrel inlet, and the thermally-lined transition section to the launch tube.

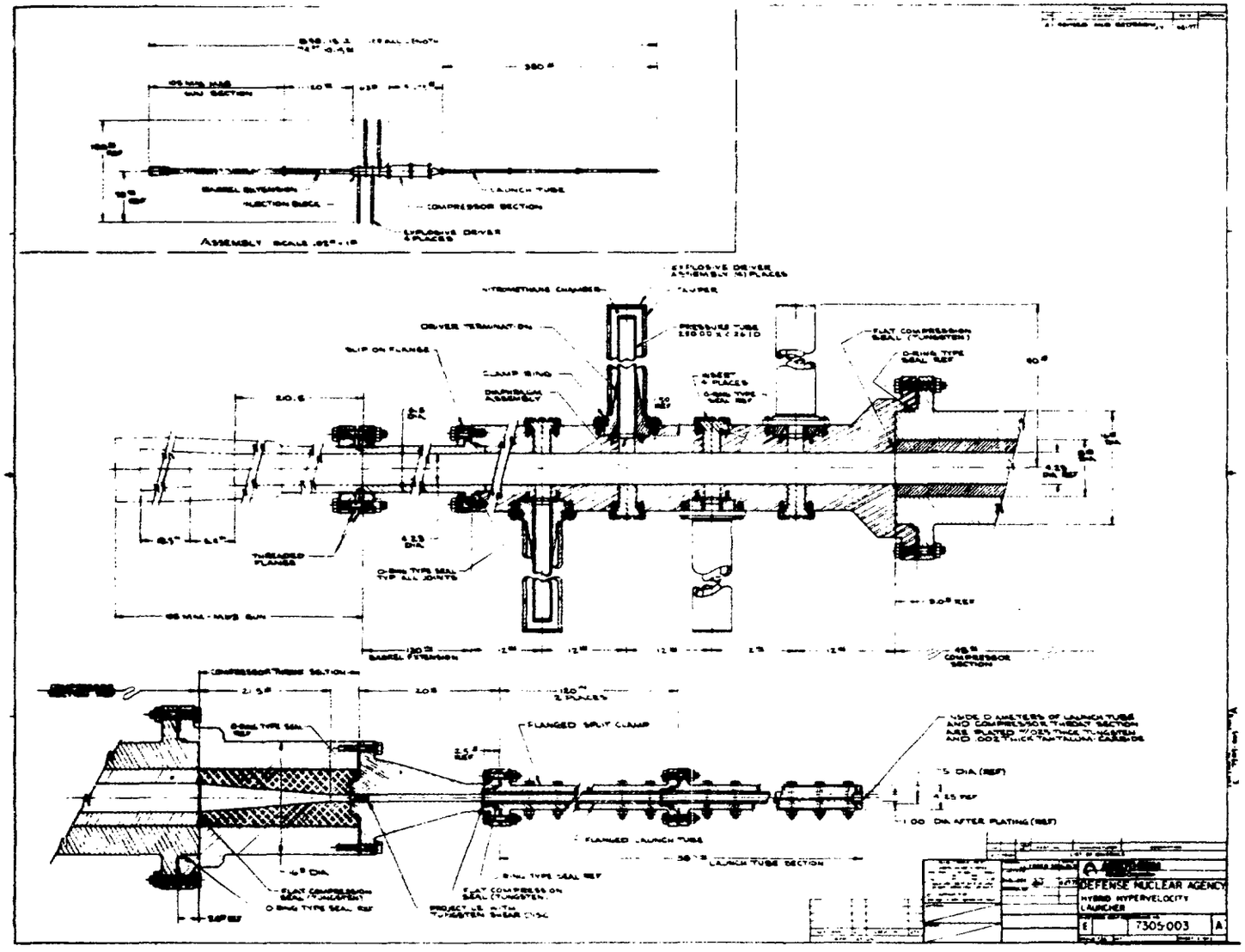

Figure 22. 1-inch bore (1/4-scale) hybrid launcher assembly drawing.

The 400-caliber launch tube will be fully lined and will be constructed as a split block clamp for removal and replacement of thermal liners. The bore of the 1/4-scale launch tube will be 1 inch. It may be converted to a superbore mode by replacing the launch tube liner and reboring and relining the compressor [illegible] and transition sections.

The launcher will be mounted rigidly on reinforced concrete stands at an outdoor test site capable of handling up to 150 pounds of high explosives used in the drivers. The models will be fired into a short, expendable plastic range where velocity and model condition will be evaluated. Pressure transducers and thermocouples will be used to measure pressures and heat loads at selected locations in the compressor section and launch tube.

5.2 FIRST STAGE

The performance characteristics of the standard 51-caliber M68 105-mm gun are shown in Table 5. The gun will be smooth bored to a diameter of 4.25 inches and a 25-caliber extension will be added. By mixing two standard propellants of different web sizes, a continuous range of piston mass-velocity combinations can be obtained. For example, light-fast pistons (12 pounds up to 5800 fps) and heavy-slow pistons (33 pounds up to 3500 fps) can be selected.

The extended M68 will have more performance capability than will be required and can be operated at peak combustion chamber pressures considerably lower than the working maximum (60600 psi). This will extend the lifetime of the M68 barrel considerably.

A polyethylene cylinder will be used as the first stage piston. The polyethylene will be backed by a DELRIN obturator which in addition to providing obturation has the mechanical properties to give a consistent shot-start condition.

5.3 DRIVERS AND INJECTION BLOCK

The explosive drivers that will be used in the 1/4-scale launcher tests are of proven design. Each of the four drivers will use 35 pounds of nitromethane. This design was chosen for the 1/4-scale tests to provide reliable performance with a minimum of redesign and testing. It is not intended to be scaled and used in the full-scale launcher. For this, a more efficient driver design will be evolved.

TABLE 5. PERFORMANCE CHARACTERISTICS OF THE M68 105-MM GUN
(From Reference 12)

Barrel length	51 calibers
Maximum diameter	4.224 inches
Minimum diameter	4.134 inches
Maximum service pressure	71100 psi

Propellant Weight (lbs)	Propellant Type	Projectile Weight (lbs)	Muzzle Velocity (fps)	Maximum Breech Pressure (psi)
12.26	M30 0.046 web	12.8	4850	58700
11.45	M30 0.052 web	22.72	3850	60600
11.41	M30 0.052 web	22.35	3850	59300
11.53	M30 0.052 web	22.35	3850	58300
9.18	M6 0.049 web	30.80	2700	39000
6.05	M1 0.034 web	24.80	2400	24600

The driver termination, like the driver itself, will be expendable. The taper section of the termination block is designed to collapse and form a tight seal to contain high pressure, high temperature hydrogen. This seal does not have to be perfect, since it is only required for a few hundred microseconds until the piston closes off the injection ports. The main body of the driver termination which interfaces with the injection block will not deform and can be easily unbolted from the injection block after the shot.

The injection block is massive and designed to be reusable. The outside of the injection block is rectangular to facilitate driver attachment. The inside of the injection block will not be lined since the expected thermal loads can be handled by steel. Replaceable rods will be installed opposite the injection ports in anticipation of damage from the transient impact of driver gas at injection. The injection block is designed to accommodate peak pressures of 3.5 kilobars.

Details of the explosive driver, driver termination and injection port are shown in Figure 23.

5.4 COMPRESSOR SECTION

The compressor is divided into three sections for disassembly and inspection of thermal liners and model.

The upstream section is unlined and fabricated as a two-piece shrink-fit assembly for maximum strength. This section is designed to hold 8 kilobars working pressure with a safety factor of 1.6 after autofrettage.

The throat section is also a two-piece shrink fit assembly. The throat nozzle has an 8° included angle for a smooth transition to the barrel and also for absorbing an accidental impact from the piston should two or more drivers fail to initiate. The throat will be lined by chemical vapor deposition of a 0.064-cm layer of tungsten overlain by a 0.005-cm layer of tantalum carbide. The entire throat section will be shipped for chemical vapor deposition of the liner to avoid the mechanical difficulties of installation and removal of a separate, replaceable liner.

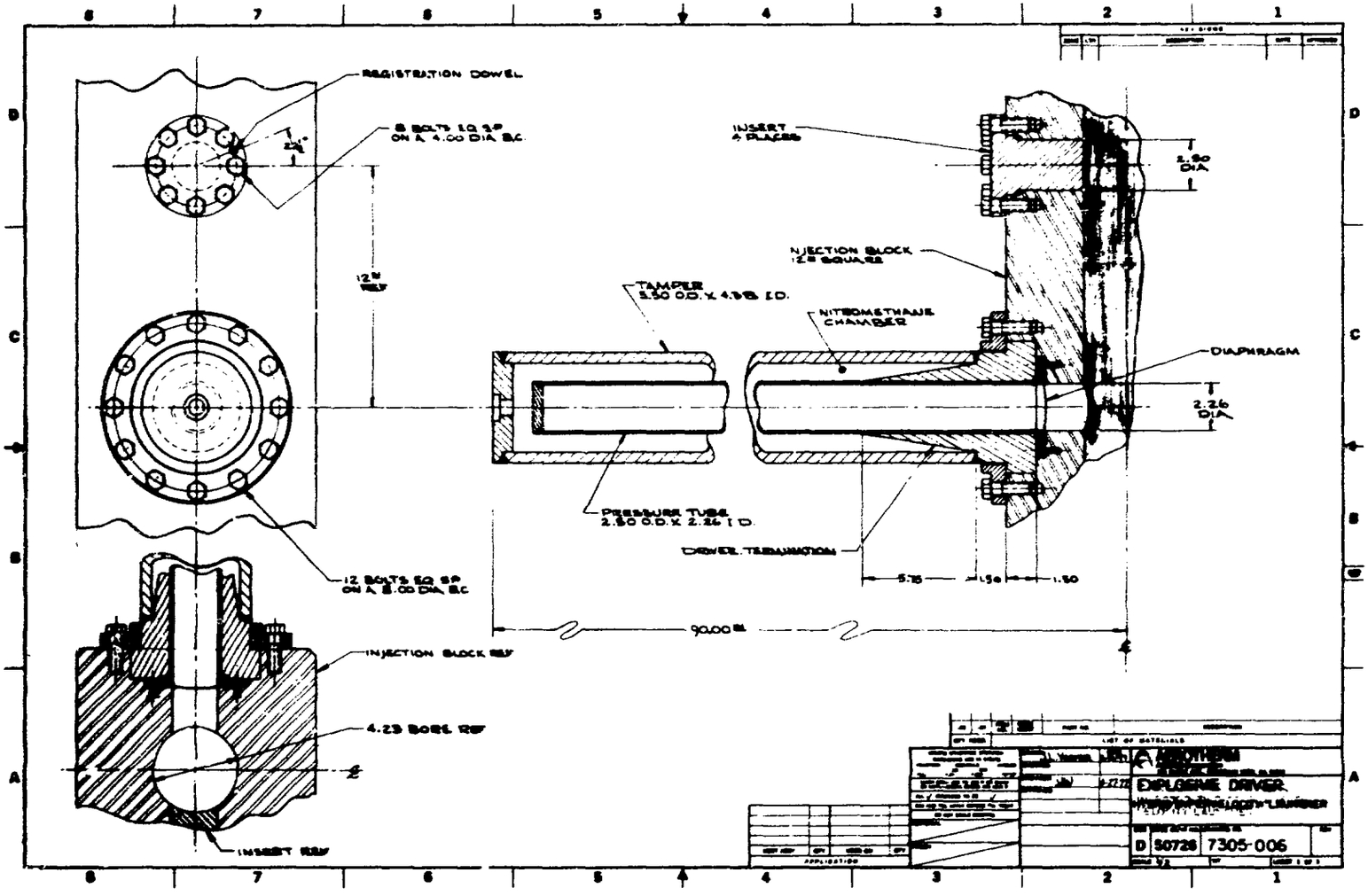

Figure 23. The explosive drivers and injection block subassembly.

The transition section which couples the throat section to the launch tube will be lined with a tungsten, tantalum carbide surface in a similar manner. All three sections will be bolted together and utilize compressed tungsten rings for sealing. These will be backed by conventional O-rings.

The model will be held in position between the throat and transition section by a thin tungsten shear disc. Tungsten is used to prevent melting in this critical region of heat transfer. The shear disc is designed to hold the model against a few hundred psi and is not required to provide a shot-start condition (see Section 2.4.2).

Details of the compressor throat section, transition section, and model shear disc are shown in Figure 24.

5.5 LAUNCH TUBE

The launch tube requires a thermal liner for its full length according to calculations. To facilitate alignment, inspection and replacement, the launch tube will be constructed as a split block clamp with three sections of lined thin wall tubing. In addition to being clamped circumferentially, the liners will be held in longitudinal compression to provide smooth, continuous, sealed joints.

The tungsten, tantalum carbide liner in addition to providing thermal protection is expected to have excellent resistance to wear from model friction.

The entire launch tube is designed to withstand internal pressures of 6 kilobars. Details of the launch tube design are shown in Figure 25.

5.6 TEST PROGRAM

The test program leading up to full reservoir conditions and maximum model velocities is designed to yield the maximum amount of information on the gasdynamics, heat loads, and mechanical limits of the hardware. This information, in turn, will provide the basis for the design of the full-scale launcher.

In the first series of tests, the explosive driver design will be tested and fully characterized. Very accurate measurements of shock velocity

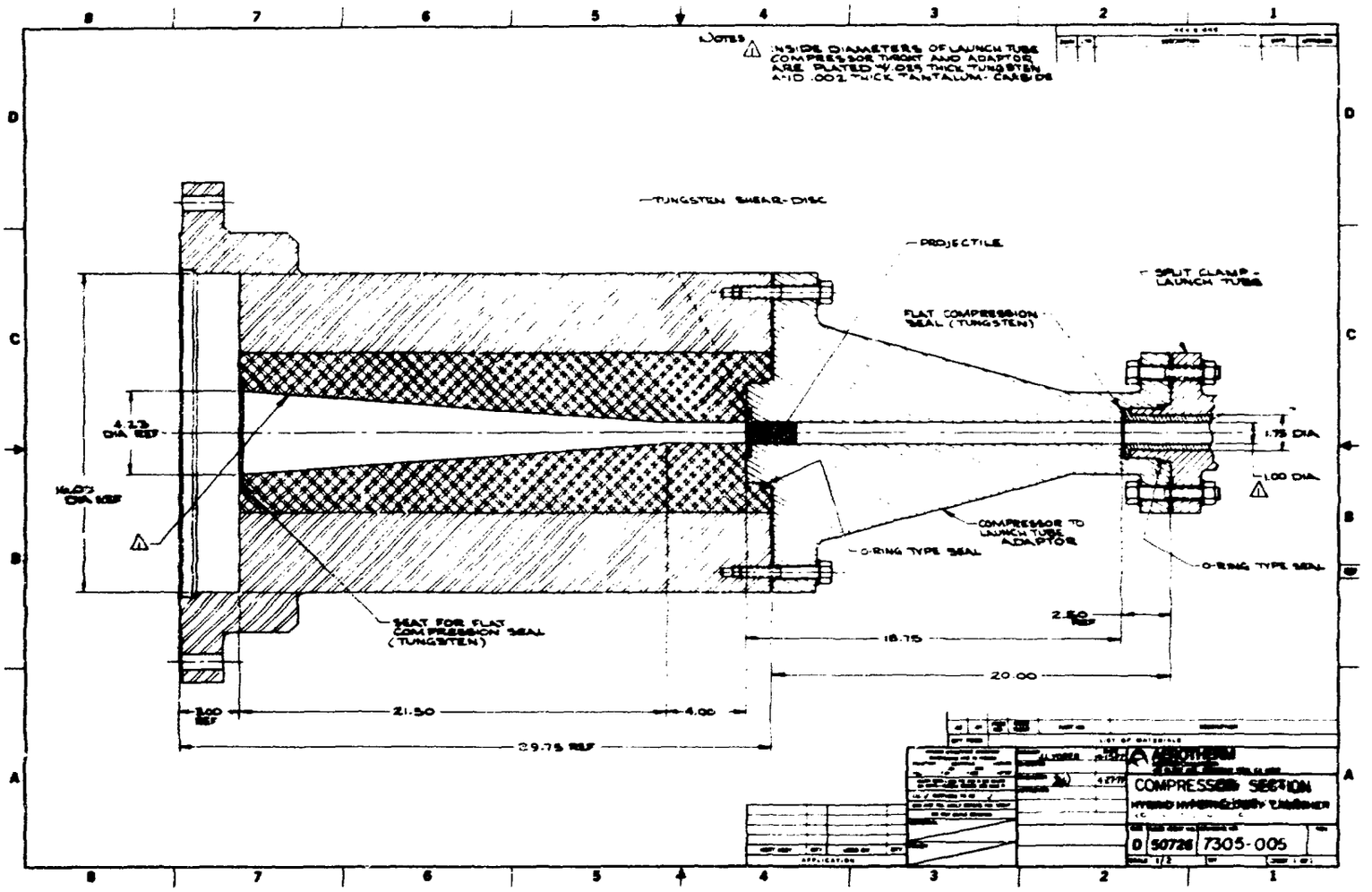

Figure 24. The compressor section subassembly.

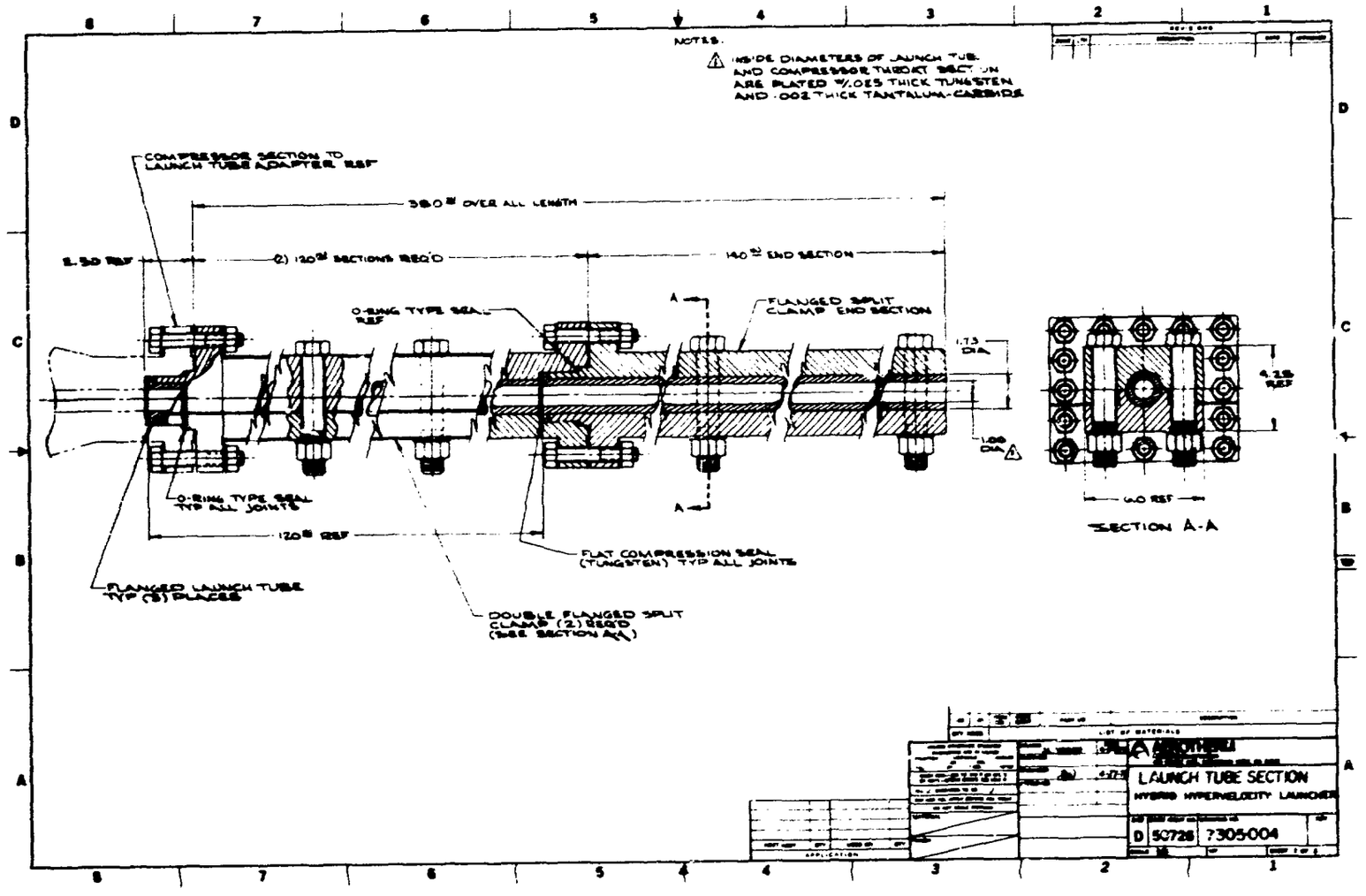

Figure 25. The launch tube subassembly.

and compression ratios will yield important information for fine tuning the hydrogen equation-of-state model for high temperatures and pressures.

In the second series of tests, drivers will be used to inject gas into a closed chamber. These tests will be used to evaluate the driver termination design, measure injection pressure histories, and accurately determine the fraction of driver gas injected. The results of these tests will be used to determine the final driver length required to inject the correct mass of hydrogen into the compressor.

Concurrently, the performance characteristics of the smooth bored extended barrel M68 will be evaluated. These tests will include proof tests of the piston sensing technique. Accurate sensing of the piston is necessary for precise control of explosive driver initiation time which in turn controls injection density and the compression isentrope for the ballistic cycle.

In the initial ballistic tests, the first stage will be disconnected and the upstream end of the injection block will be flanged off. The launcher will be operated with the drivers only. These tests will give a lower performance limit and provide an evaluation of mechanical and thermal damage for the operation of the drivers only. Little damage is expected.

The first stage will then be connected and piston energy will be increased gradually over a series of tests. Response to increasingly higher compressed states will be carefully measured and observed. As higher piston energies are reached, the optimum combination of piston mass and velocity will be evolved. From calculations optimum piston velocity appears to be between 4500 fps and 5200 fps. These tests will culminate with a demonstration of full reservoir conditions and maximum model velocity.

SECTION 6

CONCLUSIONS

This contract was undertaken to recommend the best approach for launching high-β models to reentry velocities in a ground-based facility. Specifically, the best means were sought for accelerating a 4-inch diameter fragile model weighing 10 to 12 pounds to a velocity of 20000 fps. The conclusions reached in this effort are:

- The hybrid two-stage launcher is the most practical means of achieving the required performance for fragile high-β models
- Peak reservoir pressure, temperature and rate of pressure buildup can all be controlled independently in the hybrid launcher ballistic cycle so that design performance can be achieved within the mechanical and thermal constraints of the launcher and model
- The key to the hybrid launcher concept is the use of explosive drivers to precondition and inject hydrogen into the compressor section of a two-stage gun. This leads to high-energy reservoir states unattainable with conventional two-stage guns of practical size.
- Several small high pressure explosive drivers in a simple injection arrangement are used to accurately control the injection of gas into the compressor section
- The key to utilizing the high energy/high temperature reservoir states in the hybrid launch cycle is the use of tungsten, tantalum carbide liners throughout the throat section and launch tube

- A hybrid two-stage launch cycle has been designed to launch a 4-inch diameter, 10-pound model to 6.1 km/sec with adequate margin for losses and without exceeding 5 kilobars on the model or melting the interior of the launcher
- The peak reservoir pressures and temperatures may be relaxed and the launch mass of the model increased by saboting the model and using a "superbored" launch tube
- For even higher model mass or velocity, the performance range of the hybrid launcher can be extended by superboring and/or injection of additional high energy gas along the launch tube
- The design of hardware for a 1/4-scale hybrid launcher has been completed. The 1-inch diameter launch tube can be converted to a 1-1/4-inch diameter superbore by minor modifications to the compressor throat and launch tube liner.

SECTION 7

RECOMMENDATIONS

Several hybrid two-stage ballistic cycle options have been considered under this contract. Within the specified design constraints, these options satisfy performance requirements with adequate allowances for losses. Two key design problems have been analyzed and solved. A design and configuration of explosive drivers has been developed that avoids gas injection difficulties. A thermal liner strategy has been devised that will handle heat loads during compression without melting. As a result, the following actions are recommended:

- The 1/4-scale hybrid launcher design developed under this contract should be built and tested
- Long-range planning on items substantially affecting the cost of the full-scale hybrid launcher should be initiated. These items include: test site selection; availability of 16-inch smooth-bore gun for the first stage; availability of alloy steel and selection of fabricators.
- Long-range planning should begin to integrate a full-scale hybrid launcher system into a free-flight or track-guided test facility and to evaluate the special problems associated with the use of explosive drivers
- A detailed study should be made of the feasibility of coupling a superbore launcher with a track-guided range. A trade-off must be made between the extended performance range of the superbore launcher and the problems associated with sabot stripping.

REFERENCES

1. Seifert, K., "Hypervelocity Launcher Design," PIFR-708, Final (Draft) Report prepared for DNA by Physics International Company, December 1975.

2. Cohen, L. M., et al., "Feasibility of a Hybrid Hypervelocity Launcher," Aerotherm Final Report No. TR-77-238, January 1977.

3. Seigel, A. E., "The Theory of High Speed Guns," AGARDograph 91, prepared by North Atlantic Treaty Organization Advisory Group for Aerospace Research and Development, May 1965.

4. Hofmann, R., "STEALTH: A Lagrange Explicit Finite Difference Code for Solids, Structural and Thermohydraulic Analysis," EPRI Technical Report NP-176 Project 307, June 1976.

5. Wool, M. R., "User's Manual Aerotherm Charring Material Thermal Response and Ablation Program, Version 3," Aerotherm Report No. UM-70-14 prepared for the Air Force Rocket Propulsion Laboratory, April 1970.

6. Dahm, T. J. and Anderson, L. W., "Propellant Gas Convective Heat Transfer in Gun Barrels," Aerotherm Final Report No. 70-18, August 1970.

7. Colburn, A. P., "A Method of Correlating Forced Convection Data and a Comparison with Fluid Friction," Transaction — American Institute of Chemical Engineers, p. 174, 1933.

8. Handbook of Chemistry and Physics, 36th Edition, Chemical Rubber Publishing Company, September 1954.

9. Holzl, R. A., Chemetal Corporation, private communication, March 1977.

10. Baum, D. W., et al., "Feasibility of Explosively-Driven Hypervelocity Projectiles," Final Report 109, ARTEC Associates, Hayward, California, March 1974.

11. Watson, J. D., "A Summary of the Development of Large Explosive Guns for Reentry Simulation," PIFR-155, Final Report prepared for ARPA by Physics International Company, August 1970.

12. Anderson, H. B., "Artillery Ammunition Master Calibration Chart," Report Number 1375, 14th Revision, Aberdeen Proving Ground, November 1971.

APPENDIX A

SUMMARY OF STEALTH CODE BALLISTIC CYCLE CALCULATIONS

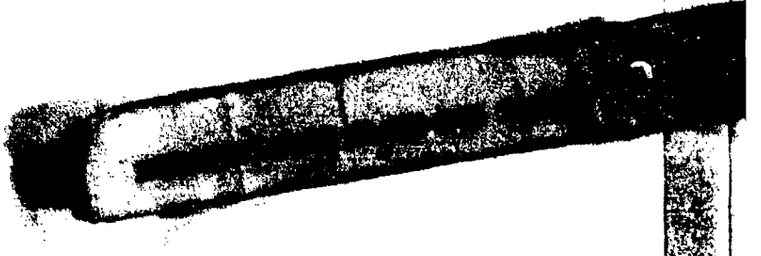

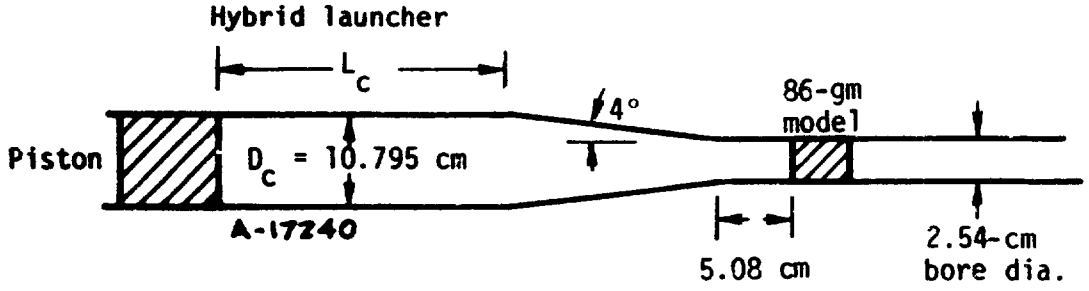

- Real hydrogen equation-of-state used unless noted
- Gas initially at rest and evenly distributed unless noted
- Maximum reservoir pressures and temperatures taken upstream of the compressor throat

Run No.	Pist. Mass (lbs)	Pist. Vel. (fps)	L_c/D_c	G/M	Total Energy (e.u.)	p_{max} Res. (kb)	T_{max} Res. (°K)	p_{max} Model (kb)	u_{300} (km/sec)	u_{350} (km/sec)	Shot Start (kb)	Gas Zones
1	10.78	5000	25	2	156	7.0	5600	5.1	5.77	6.15	0	35
2	10.78	5500	25	2	168	8.9	5810	6.6	6.46	6.83	0	35
3	10.78	6000	25	2	181	11.8	6100	8.6	7.18	7.55	0	35
4	10.78	5000	25	1.5	131	7.6	5870	6.1	6.12	6.44	0	35
5	10.78	5000	20	2	156	8.2	5580	7.0	6.30	6.60	0	57
6	12	4850	25	2	159	7.3	5640	5.1	5.80	6.21	0	35
7	15.52	5000	25	2	181	11.1	6020	7.1	6.89	7.37	0	35
8	22	3500	25	2	156	6.4	5490	4.0	5.24	5.66	0	35
9	22	3850	25	2	168	8.0	5710	4.8	5.77	6.26	0	35
10	22	4000	25	2	173	8.7	5780	5.2	6.03	6.52	0	35
11	22	4200	25	2	181	10.5	5970	5.8	6.38	6.90	0	35
12	22	3500	20	2	156	7.3	5460	5.2	5.85	6.26	0	57
13	22	3850	20	2	168	9.3	5690	6.4	6.43	6.92	0	57
14	26.62	3500	25	2	168	7.7	5660	4.3	5.47	6.00	0	35
15	26.62	3500	20	2	168	8.8	5640	5.6	6.16	6.64	0	57

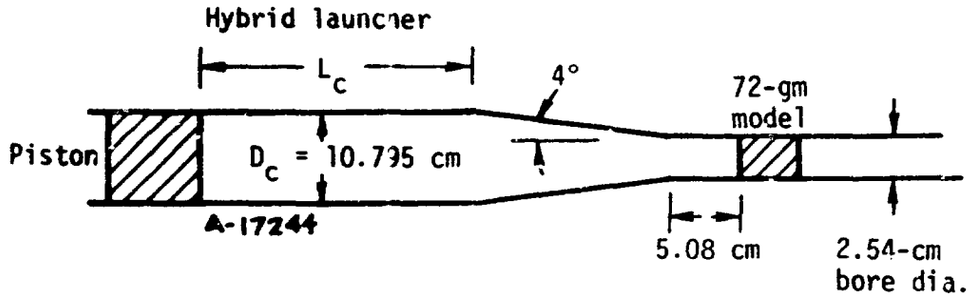

- Real hydrogen equation-of-state used unless noted
- Gas initially at rest and evenly distributed unless noted
- Maximum reservoir pressures and temperatures taken upstream of the compressor throat

Run No.	Pist. Mass (lbs)	Pist. Vel. (fps)	L_c/D_c	G/M	Total Energy (e.u.)	p_{max} Res. (kb)	T_{max} Res. (°K)	p_{max} Model (kb)	u_{300} (km/sec)	u_{350} (km/sec)	Shot Start (kb)	Gas Zones
16	10.78	5000	25	2.4	156	6.5	5510	4.6	6.06	6.46	0	35
17	10.78	5000	25	2.4	156	7.0	5710	5.6	6.26	6.57	2	35
18	10.78	5500	25	2.4	168	9.0	5840	5.6	6.76	7.14	0	35
19	10.78	5000	25	2	140	7.2	5750	4.9	6.25	6.66	0	35
20	10.78	5000	25	2	140	6.7	5540	5.4	6.44	6.77	2	35
21	10.78	5000	25	2	140	6.4	5610	4.7	6.02	6.36	2	35[a]
22	10.78	5165	25	2	144	7.8	5820	5.3	6.49	6.91	0	35
23	11.5	5000	25	2	144	7.8	5810	5.1	6.44	6.87	0	35
24	11.5	5000	25	2	144	8.0	5840	6.1	6.50	7.00	0	70
25	11.5	5000	25	2	144	6.3	5760	6.3	6.00	6.43	0	35[b]
26	11.5	5000	25	2	144	6.8	5660	5.1	6.02	6.47	0	70[b]
27	12.5	5000	25	2	149	8.7	5930	5.5	6.71	7.16	0	35
28	22	3500	20	2.4	156	7.2	5460	4.6	5.97	6.44	0	57
29	22	3850	20	2.4	168	9.2	5680	5.4	6.53	7.08	0	57
30	22	3500	17.5	2.4	156	8.1	5480	5.3	6.35	6.85	0	51
31	26.62	3500	20	2.4	168	8.7	5630	4.8	6.21	6.77	0	57
32	26.62	3850	20	2.4	182	11.5	5910	6.1	6.90	7.48	0	57

[a]Covolume parameter b is set to 0

[b]Gas initially at rest and in the first 14.2 diameters of the compressor

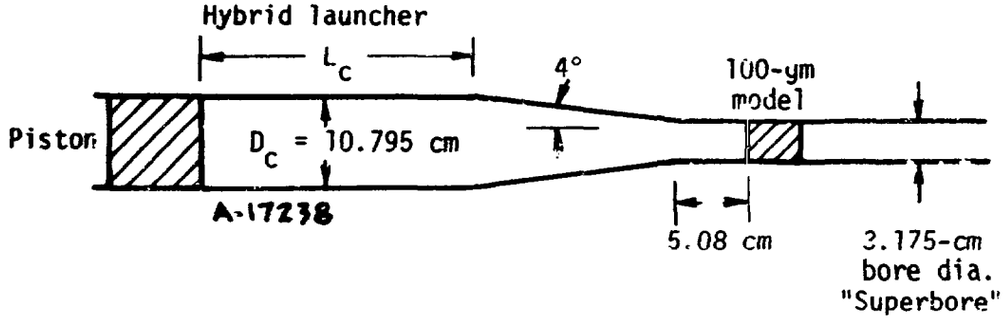

- Real hydrogen equation-of-state used unless noted
- Gas initially at rest and evenly distributed unless noted
- Maximum reservoir pressures and temperatures taken upstream of the compressor throat

Run No.	Pist. Mass (lbs)	Pist. Vel. (fps)	L_c/D_c	G/M	Total Energy (e.u.)	p_{max} Res. (kb)	T_{max} Res. (°K)	p_{max} Model (kb)	u_{300} (km/sec)	u_{350} (km/sec)	Shot Start (kb)	Gas Zones
33	12.5	5000	25	1.75	167	7.1	5580	4.3	6.96	7.40	0	35
34	12.5	5100	25	1.75	169	7.3	5510	4.7	7.00	7.41	0	35
35	13	5000	30	2.25	198	6.5	5450	3.8	6.49	6.85	0	41
36	14	5000	30	2.25	203	6.9	5500	3.9	6.61	6.99	0	41

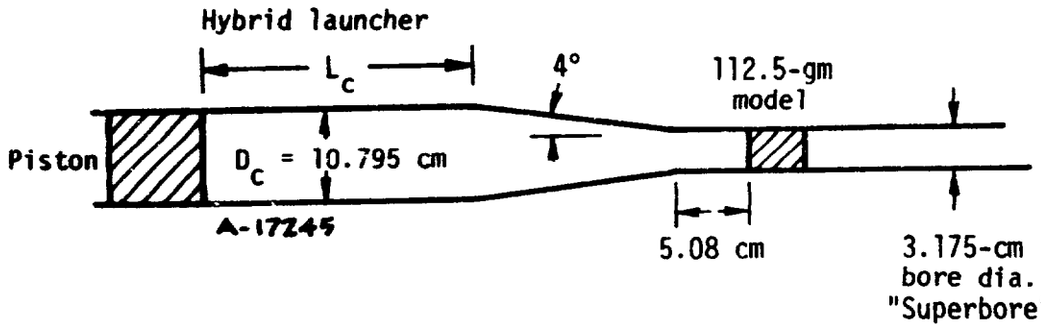

- Real hydrogen equation-of-state used unless noted
- Gas initially at rest and evenly distributed unless noted
- Maximum reservoir pressures and temperatures taken upstream of the compressor throat

Run No.	Pist. Mass (lbs)	Pist. Vel. (fps)	L_c/D_c	G/M	Total Energy (e.u.)	p_{max} Res. (kb)	T_{max} Res. (°K)	p_{max} Model (kb)	u_{300} (km/sec)	u_{350} (km/sec)	Shot Start (kb)	Gas Zones
37	13	4800	25	1.56	164	6.6	5510	4.7	6.61	7.01	0	35
38	13	5000	25	1.56	169	7.5	5630	5.0	6.92	7.30	0	35
39	14	5000	25	1.56	175	8.1	5710	5.3	7.14	7.55	0	35
40	13	5000	30	2.00	198	6.9	5500	4.2	6.25	6.63	0	41
41	14	5000	30	2.00	204	6.8	5480	4.4	6.38	6.83	0	41
42	13	4800	25	1.56	164	7.2	7100	4.5	5.98	6.37	0	40[a]

[a]60 percent of gas at 0.957 e.u./gm is initially in the first 14 diameters of the compressor and 40 percent of gas at 0.068 e.u./gm is in the remainder.

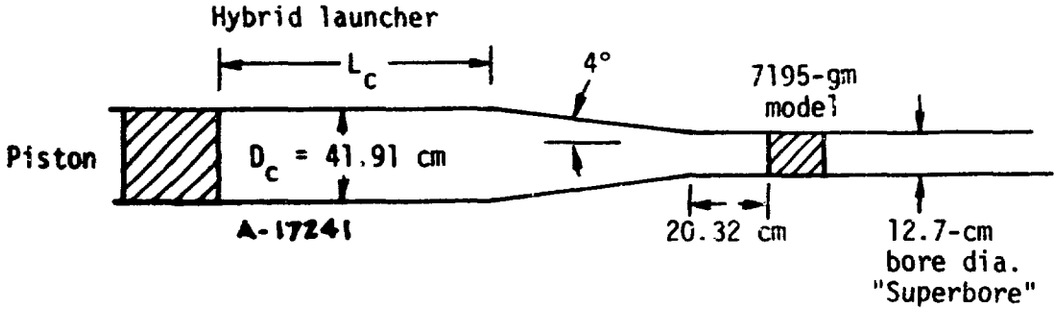

- Real hydrogen equation-of-state used unless noted
- Gas initially at rest and evenly distributed unless noted
- Maximum reservoir pressures and temperatures taken upstream of the compressor throat

Run No.	Pist. Mass (lbs)	Pist. Vel. (fps)	L_c/D_c	G/M	Total Energy (e.u.)	p_{max} Res. (kb)	T_{max} Res. (°K)	p_{max} Model (kb)	u_{300} (km/sec)	u_{350} (km/sec)	Shot Start (kb)	Gas Zones
43	832	4800	25.8	1.56	10492	6.8	5490	5.4	6.67	7.08	0	70
44	801	4800	25.8	1.56	10332	6.9	5500	5.3	6.54	6.96	0	70

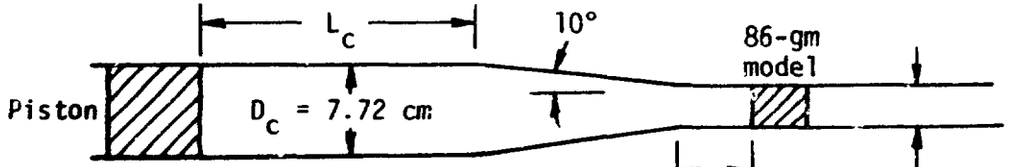

"Best" PI configuration, see Reference 1.

Run No.	Pist. Mass (lbs)	Pist. Vel. (fps)	L_c/D_c	G/M	Total Energy (e.u.)	p_{max} Res. (kb)	T_{max} Res. (°K)	p_{max} Model (kb)	u_{300} (km/sec)	u_{350} (km/sec)	Shot Start (kb)	Gas Zones
45	10	3500	33.2	1.23	79	5.3	4850	3.5	5.06	5.39	0	67
46	10	3500	33.2	1.23	79	5.4	6780	3.5	5.13	5.46	0	67[a]

[a]Constant γ = 1.4 gas

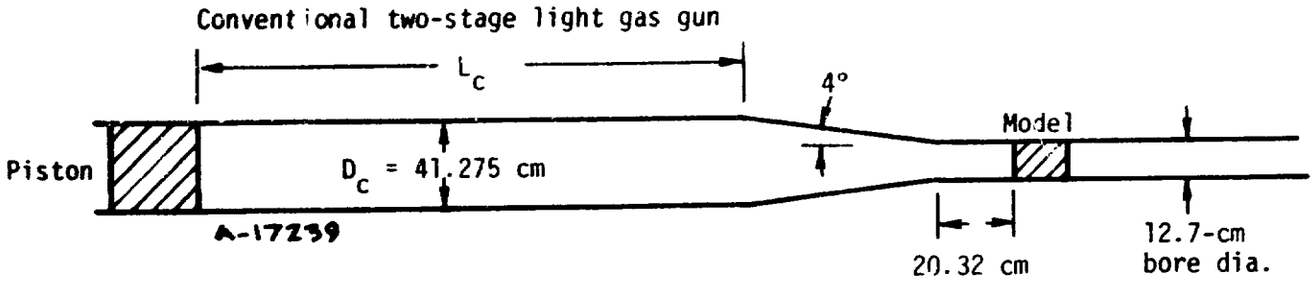

- Real hydrogen equation-of-state used unless noted
- Gas initially at rest and evenly distributed unless noted
- Maximum reservoir pressures and temperatures taken upstream of the compressor throat

Run No.	Model Mass (gm)	Pist. Mass (lbs)	Pist. Vel. (fps)	L_c/D_c	G/M	Total Energy (e.u.)	P_{max} Res. (kb)	T_{max} Res. (°K)	P_{max} Model (kb)	u_{300} (km/sec)	u_{350} (km/sec)	Shot Start (kb)	Gas Zones
47	5448	900	5000	161	2.0	6300	—	—	—	—	—	2	101
48	5448	900	5000	161	1.0	6100	—	—	—	—	—	2	101
49	4058	670	5000	161	1.4	4550	22.0	1080	14.5	—	—	2	34
50	4058	670	5000	161	5.6	5300	12.5	1770	8.3	8.2	—	2	34
51	4058	670	5000	161	8.4	5900	9.7	1500	9.0	6.8	—	2	34

DISTRIBUTION LIST

DEPARTMENT OF DEFENSE

Director
Defense Advanced Rsch. Proj. Agency
ATTN: Strategic Tech. Office

Defense Documentation Center
Cameron Station
12 cy ATTN: TC

Director
Defense Intelligence Agency
ATTN: DT-1B
ATTN: DI-7D
ATTN: DT-2, Wpns. & Sys. Div.

Director
Defense Nuclear Agency
ATTN: TISI, Archives
ATTN: DDST
ATTN: STSP
3 cy ATTN: TITL, Tech. Library
3 cy ATTN: SPAS

Commander
Field Command
Defense Nuclear Agency
ATTN: FCPR

Director
Joint Strat. Tgt. Planning Staff, JCS
ATTN: JLTW-2
ATTN: JPTM

Chief
Livermore Division Fld. Command, DNA
Lawrence Livermore Laboratory
ATTN: FCPRL

OJCS/J-5
ATTN: J-5, Plans & Policy Nuc. Div.

Under Secretary of Def. for Rsch. & Engrg.
ATTN: S&SS (OS)
ATTN: AD/ET, J. Persh

DEPARTMENT OF THE ARMY

Director
BMD Advanced Tech. Ctr.
Huntsville Office
ATTN: ATC-T, Melvin T. Capps

Program Manager
BMD Program Office
ATTN: Technology Division

Commander
BMD System Command
ATTN: BMDSC-TB, R. Simpson

Dep. Chief of Staff for Rsch. Dev. & Acq.
ATTN: NCB Division

Deputy Chief of Staff for Ops & Plans
ATTN: Dir. of Chem. & Nuc. Ops.

DEPARTMENT OF THE ARMY (Continued)

Commander
U.S. Army Missile Command
ATTN: DRSMI-XS, Chief Scientist

Commander
Harry Diamond Laboratories
ATTN: DRXDO-RBH
ATTN: DRXDO-RC
ATTN: DRXDO-NP

Commander
Picatinny Arsenal
ATTN: SARPA-ND-C-T
ATTN: SMUPA-MD

Director
U.S. Army Ballistic Research Labs.
ATTN: Robert E. Eichelberger

Commander
U.S. Army Mat. & Mechanics Rsch. Ctr.
ATTN: DRXMR-HH

Commander
U.S. Army Materiel Dev. & Readiness Cmd.
ATTN: DRCDE-D

Commander
U.S. Army Nuclear Agency
ATTN: MONA

DEPARTMENT OF THE NAVY

Chief of Naval Operations
ATTN: OP, 604F4

Director
Naval Research Laboratory
ATTN: Code 2600, Tech. Library

Commander
Naval Sea Systems Command
ATTN: Code 0351

Officer-In-Charge
Naval Surface Weapons Center
ATTN: Code WA-07
2 cy ATTN: Code WA43

Director
Strategic Systems Project Office
ATTN: NSP-272
ATTN: Fred Wimberly

DEPARTMENT OF THE AIR FORCE

Commandant
AF Flight Dynamics Laboratory, AFSC
ATTN: FXG

AF Geophysics Laboratory, AFSC
ATTN: Chan Touart

DEPARTMENT OF THE AIR FORCE (Continued)

AF Materials Laboratory, AFSC
ATTN: MXS
ATTN: MBE
ATTN: LTM
ATTN: MBC

AF Office of Scientific Research
ATTN: Paul Thurston

AF Rocket Propulsion Laboratory, AFSC
ATTN: RTSN

AF Weapons Laboratory, AFSC
ATTN: DYV
ATTN: SUL

Headquarters
Air Force Systems Command
ATTN: DLCAM

Commander
Arnold Engineering Development Center
ATTN: XOA

Commander
Foreign Technology Division, AFSC
ATTN: PDBG

Headquarters USAF/RD
ATTN: RDQ
ATTN: RDQSM

SAMSO/DY
ATTN: DYS

SAMSO/MN
ATTN: MNNR
ATTN: MNNH

SAMSO/RS
ATTN: RST
ATTN: RSS
ATTN: RSSR
7 cy ATTN: RSSE

Commander In Chief
Strategic Air Command
ATTN: XOBM
ATTN: NRI
ATTN: DOXT

DEPARTMENT OF ENERGY

University of California
Lawrence Livermore Laboratory
ATTN: C. Joseph Taylor, L-92
ATTN: G. Staihle, L-24
ATTN: Larry W. Woodruff, L-96
ATTN: Charles S. Godfrey

Los Alamos Scientific Laboratory
ATTN: Doc. Control for J. W. Taylor

DEPARTMENT OF ENERGY (Continued)

Sandia Laboratories
Livermore Laboratory
ATTN: Doc. Control for T. Gold

Sandia Laboratories
ATTN: Doc. Control for R. Clem
ATTN: Doc. Control for D. Rigali
ATTN: Doc. Control for A. W. Synder
ATTN: Doc. Control for Albert Chabai

DEPARTMENT OF DEFENSE CONTRACTORS

Acurex Corporation
ATTN: K. Seifert
ATTN: J. Courtney
ATTN: J. Huntington
ATTN: J. D. Watson
ATTN: T. J. Dahm
ATTN: A. D. Anderson

Aerojet Liquid Rocket Company
ATTN: R. Jenkins

Aeronautical Rsch. Assoc. of Princeton, Inc.
ATTN: Coleman Donaldson

Aerospace Corporation
ATTN: D. H. Platus
ATTN: R. Mortensen
ATTN: D. T. Nowlan
ATTN: H. F. Dyner
ATTN: W. Barry
ATTN: D. Geiler
ATTN: Wallis Grabowsky
ATTN: R. Hallse
ATTN: R. H. Palmer
ATTN: P. Legendre
ATTN: W. Portenier
ATTN: M. Gyetvay

ARO, Incorporated
ATTN: John C. Adams
ATTN: Glenn Norfleet

AVCO Research & Systems Group
ATTN: William Broding
ATTN: John E. Stevens, J100
ATTN: George Weser

Battelle Memorial Institute
ATTN: Technical Library

The Boeing Company
ATTN: Brian Lempriere

Brown Engineering Company, Inc.
Cummings Research Park
ATTN: Ronald Patrick

Calspan Corporation
ATTN: M. S. Holden

DEPARTMENT OF DEFENSE CONTRACTORS (Continued)

Effects Technology, Inc.
ATTN: Robert Wengler

Ford Aerospace & Communications Operations
ATTN: A. Demetriades

General Electric Company
Space Division
Valley Forge Space Center
ATTN: B. M. Maguire
ATTN: Phillip Cline
ATTN: A. Martellucci

General Electric Company
TEMPO-Center for Advanced Studies
ATTN: DASIAC

General Research Corporation
ATTN: Robert E. Rosenthal

Institute for Defense Analyses
ATTN: Joel Bengston
ATTN: IDA, Librarian, Ruth S. Smith

ION Physics Corporation
ATTN: Robert D. Evans

Kaman Sciences Corporation
ATTN: Thomas Meagher
ATTN: Frank H. Shelton

Lockheed Missiles & Space Co., Inc.
ATTN: Charles M. Lee
ATTN: Gerald T. Chrusciel
ATTN: Donald A. Price
ATTN: Robert Au

Lockheed Missiles and Space Co., Inc.
ATTN: T. R. Fortune

Martin Marietta Corporation
Orlando Division
ATTN: James M. Potts, MP-61
ATTN: William A. Gray, MP-61
ATTN: Laird Kinnaird

McDonnell Douglas Corporation
ATTN: L. Cohen
ATTN: R. J. Reck
ATTN: H. Hurwicz

National Academy of Science
ATTN: National Materials Advisory Board for
Donald G. Groves

Pacific-Sierra Research Corp.
ATTN: Gary Lang

Physical Sciences, Inc.
ATTN: M. S. Finson

Physics International Company
ATTN: Doc. Control for James Shea

DEPARTMENT OF DEFENSE CONTRACTORS (Continued)

Prototype Development Associates, Inc.
ATTN: L. Hudack
ATTN: J. E. Dunn

R & D Associates
ATTN: Raymond F. Ross
ATTN: F. A. Field
ATTN: Paul Rausch

Science Applications, Inc.
ATTN: John Warner

Science Applications, Inc.
ATTN: George H. Burghart
ATTN: Ken Kratch

Science Applications, Inc.
ATTN: K. Kratch
ATTN: Lyle Dunbar
ATTN: Carl Swain

Southern Research Institute
ATTN: C. D. Pears

Spectron Development Laboratories
ATTN: T. Lee

SRI International
ATTN: Donald Curran
ATTN: George R. Abrahamson

Systems, Science and Software, Inc.
ATTN: G. A. Gurtman

TRW Defense & Space Sys. Group
ATTN: W. W. Wood
ATTN: D. H. Baer, R1-2136
ATTN: I. E. Alber, R1-1008
ATTN: Thomas G. Williams
ATTN: A. W. Zimmerman

TRW Defense & Space Sys. Group
San Bernardino Operations
ATTN: E. Y. Wong, 527/712
ATTN: V. Blankenship
ATTN: William Polich
ATTN: Earl W. Allen, 520/141
ATTN: L. Berger